Load models for reliability analysis of six dike sections along the Westerschelde

C.F. de Valk

Advisory and Research Group on
Geo Observation Systems and Services

Document status sheet

Title	: Load models for reliability analysis of six dike sections along the Westerschelde
Code	: RP_A95
Date	: 5 November 1998
Status	: Final
Issue	: 1.0
Contractnr	: RKZ_517
Projectnr	: A95
Prepared for	: Rijkswaterstaat National Institute for Coastal and Marine Management/RIKZ
Author	: _____ C.F. de Valk
Approved by	: _____ P. Groenewoud
Distribution	: Rijkswaterstaat National Institute for Coastal and Marine Management/RIKZ J.G.A. van Marle Alkyon G.Ph. van Vledder

Executive summary

This report presents a probabilistic model for hydraulic loads on the dikes on the Westerschelde estuary, and the application of this model to analyse the reliability of these dikes as well the nearshore climate.

The failure mechanisms considered are wave overtopping or wave run-up, and instability of a top layer consisting of blocks of concrete or stone. The load on the structure is expressed as a function of still water level (SWL), significant wave height, peak wave period and mean wave direction at the toe of the dike or seawall. The six coastal sites considered in this study are shown in Figure 12. This map shows that all sites are located at least 10 km from the inlet, so the direct effect of waves propagating from the North Sea is limited. Therefore, the wave parameters at the coastal sites are primarily determined by wind speed and direction, and by local SWL. The diagram below summarises the situation.

input variables	output variables
SWL at *Vlissingen*	SWL *near structure*
windspeed at *Vlissingen*	significant wave height *near structure*
wind direction at *Vlissingen*	peak period *near structure*
	mean wave direction *near structure*

The wave modelling is reported in the accompanying Alkyon report [Van Vledder, 1998] in Dutch. In this report, other aspects are discussed such as the statistics of the input variables, the sea level variation within the estuary, the parametric representation of the wave transformations derived from the wave model results, the dike sections and failure mechanisms, and the reliability analysis method.

The reliability analysis is made using a semi-parametric extreme value method described in [De Valk et al., 1998] which has been extended to deal with marginal return periods which depend on wind or wave direction. The method is implemented in a new version 2.2 of the software program DPViewer. In addition, an extension of the method is discussed to include the effects of uncertainties in climate, models and structure into the reliability analysis.

Main findings of the study are the following.

- Overall, the marginal fits of wind speed and SWL at Vlissingen made for 12 wind direction sectors seem to match the data rather well. As a function of wind direction, all parameters vary smoothly for both wind speed and for SWL. Only the wind speed marginals for certain directions may need some improvement by correcting the data for local disturbances of the wind profile.

- Wind speed and SWL coinciding with SWL maxima appear to be *asymptotically dependent* (a strong form of dependence) for wind directions in 225°-345°.
- This is good enough in practice to allow application of a semi-parametric method for estimating return periods of failure which is based on directional marginals. The results of this method look promising.
- In particular, the variation of marginals with wind direction appears to have a bigger impact on the near-shore wave climate and the reliability of the structure than deviation from a one-one relationship between SWL and wind speed given the wind direction.
- A local FORM-like approach to include various types of uncertainties about offshore climate, wave and sea level transformations, and the response of the structure into the semi-parametric method has been pursued further.
- It is shown how return periods of failure using this local approach can be split into factors corresponding to independent sources of uncertainty. This is relevant for reducing building cost by reducing uncertainty through additional research.
- Uncertainties can also be taken into account in estimating quantiles (values with specified return periods).

Contents

List of tables

List of figures

1 Introduction

This report presents a probabilistic model for hydraulic loads on the dikes on the Westerschelde estuary, and the application of this model to analyse the reliability of these dikes as well the nearshore climate. The reliability analysis is made using an extreme value method described in [De Valk et al., 1998] which has been extended to deal with marginal return periods which depend on wind or wave direction. The method is implemented in a new version 2.2 of the software program DPViewer. In addition, an extension of the method is discussed to include the effects of uncertainties in estimates, models and structure into the reliability analysis.

The failure mechanisms considered are wave overtopping or wave run-up, and instability of a top layer consisting of blocks of concrete or stone. The load on the structure is expressed as a function of still water level (SWL), significant wave height, peak wave period and mean wave direction at the toe of the dike or seawall. The three wave parameters are primarily determined by the wind speed and direction, and by the water depth in front of the dike, so by the local SWL. The local SWL is derived from the SWL at the reference location Vlissingen (Flushing) by a simple one-to-one transformation. Waves near the structure are mainly generated inside the estuary. Assuming a uniform wind field to the west of the line Vlissingen-Breskens, the wind is set equal to the wind at Vlissingen. To the east of this line, the wind speed is assumed to be 1 m/s lower. The wave generation and propagation are modelled by a suite of SWAN models on 2-dimensional and one-dimensional grids. The diagram below summarises the situation.

Input variabeles		**Output variables**	
SWL at *Vlissingen*	η	SWL *near structure*	η
windspeed at *Vlissingen*	u_{10}	significant wave height *near structure*	$H_{m,0}$
wind direction at *Vlissingen*		peak period *near structure*	T_p
		mean wave direction *near structure*	θ_0

The wave modelling is reported in the accompanying Alkyon report [Van Vledder, 1998] in Dutch. This report will therefore focus on other aspects, such as the statistics of the input variables, the assumed sea level variation within the estuary, the parametric representation of the wave transformations derived from the wave model results, the dike sections and failure mechanisms, and the method for reliability analysis.

2 Statistics of wind and water levels

2.1 Data and storm selection

For the present study, Rijkswaterstaat RIKZ made a data-set available of hourly wind speed, wind direction, still water level (SWL) and astronomical tidal level at Vlissingen. The data-set covers the period Jan 1, 1981 - Jan 1, 1997 so a total of 16 years.

Hourly values of surge were estimated by simply subtracting the astronomical SWL from the measured SWL. Based on the data of surge and wind speed, storm events were selected using the method of [De Valk, 1994] as uninterrupted time-intervals during which at least one variable exceeds a predetermined threshold. For both surge and wind speed, the thresholds were chosen as the values exceeded during 10% of the time. This percentage is somewhat higher than the 5% used in [De Valk, 1994] and was chosen in order to detain a reasonable number of samples for wind directions which generally correspond to relatively low wind speeds. The total number of "storm" events was 3275. The thresholds were 10.50 m/s for wind speed (exceeded in 2028 storms) and 0.29 m for surge (exceeded in 2031 storms).

2.2 Omnidirectional marginals

Omnidirectional exceedance frequencies of wind speed and still water level (SWL) in Vlissingen were taken from [Rijkoort & Wieringa, 1983] and [Philippart et al., 1995], respectively. Weibull distributions were fitted to these values by least squares. This distribution is of the form

$$\mu(a) = \mu(\omega)\, e^{-((a-p)/\sigma)^{\alpha}+(\omega/\sigma)^{\alpha}} \qquad (1)$$

with $\mu(a)$ the frequency of exceedance of the value a. The estimates of the parameters are given in the tables below. The constant p is nonzero only for SWL and represents an established increase of SWL quantiles by 0.05 m since the reference year 1985 to which [Philippart et al., 1995] applies.

parameter	value
ω	23.50 m/s
$\mu(\omega)$	0.10 storms/year
σ	5.11 m/s
α	1.4320
p	0.0
q(10,000 years)	35.11 m/s

Table 1 Parameters of Weibull approximation to wind speed marginal.

parameter	value
ω	3.4000 m
$\mu(\omega)$	0.5000 storms/year
σ	0.2714 m
α	1.0319
p	0.05 m
q(10,000 years)	5.50 m

Table 2 Parameters of Weibull approximation to SWL marginal.

Figure 1 shows a plot of the fitted exceedance frequency curve for wind speed, together with exceedance frequencies derived directly from the measured wind speed storm maxima (1/16 years for the highest sample, 2/16 years for the second highest sample, etc.); the latter have been indicated by dots. There is clearly a large difference (a factor 5 in frequency or 3 m in wind speed) between the sample curve and the curve based on [Rijkoort & Wieringa, 1983].

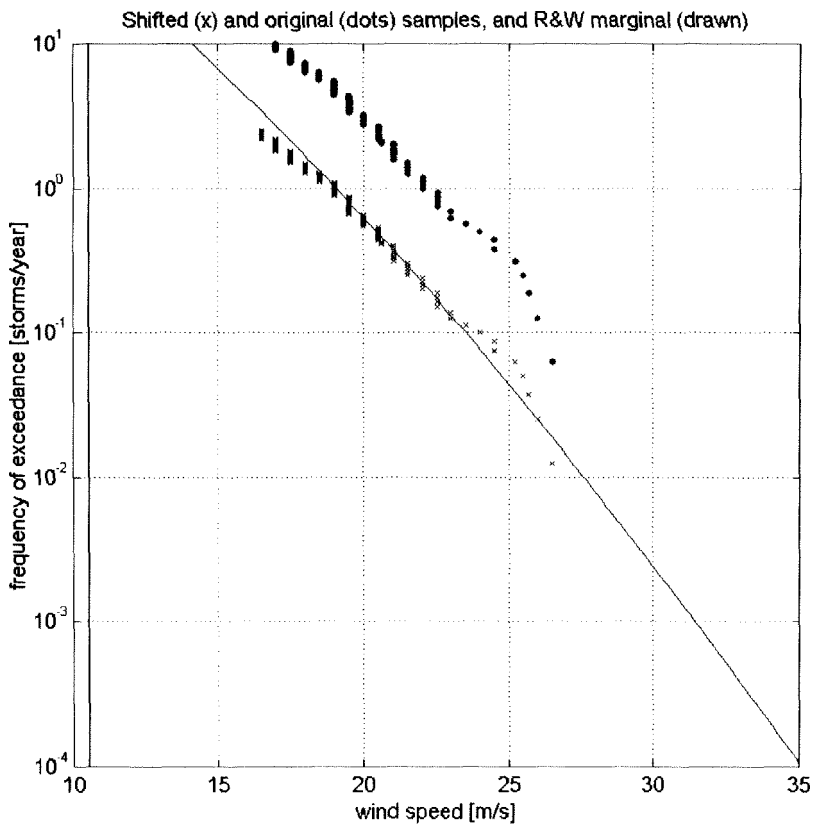

Figure 1 Exceedance frequency curve of wind speed at Vlissingen (drawn), sample exceedance frequencies (dots) and same, but reduced by factor of 5 (x).

According to KNMI (Royal Netherlands Meteorological Institute), the cause of the discrepancy is that the wind data were not collected at 10 m and have not been converted to 10 m wind, nor were the data

corrected for sheltering by terrain elements or buildings. In this study, we have simply corrected the data by reducing the sample exceedance frequencies by a factor of 5 (which gives about the same effect as decreasing wind speeds by 3 m). The resulting fit is seen in Figure 1.

A similar situation but much less drastic was encountered when plotting the sample exceedance frequencies based on the 16 year data-set with the curve derived from [Philippart et al, 1995], see Figure 2. Here, the sample exceedance frequencies were reduced by only a factor of 1.5 to fit the marginal from [Philippart et al, 1995]. Figure 2 also shows the marginal of Table 2 in which the extra increase $p = 0.05$ is incorporated (dashed line).

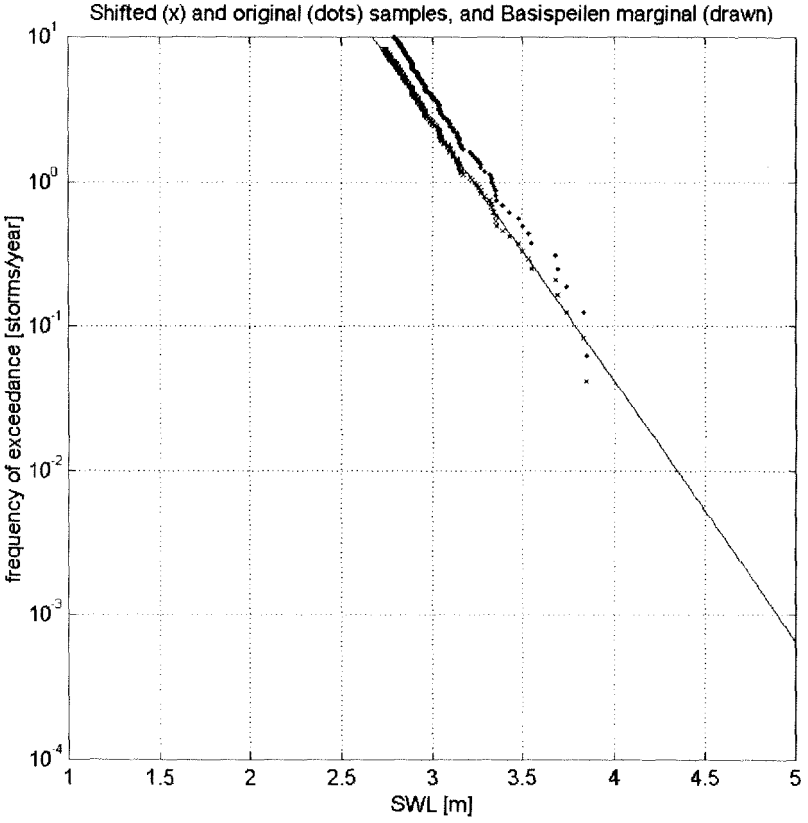

Figure 2 Exceedance frequency curve of SWL at Vlissingen (drawn) from [Philippart et al., 1995] (drawn) and increased by 0.05 m as in table 2 (dashed), sample exceedance frequencies (dots) and same, but reduced by factor of 1.5 (x).

2.3 Directional wind speed marginals

Directional marginals of wind speed were determined for the 12 sectors shown below.

Table 3 Directional sectors: their numbering, direction bounds (in nautical degrees), and corresponding colours in plots.

First, it was checked which sectors are *dominant* in the sense that the exceedance frequencies for that sector differ a constant factor from the omni-directional exceedance frequencies. Figure 3 below shows ratio's of directional exceedance frequency to omni-directional exceedance frequency derived directly from the data as a function of the number of samples taken into account. For dominant directions, the plotted ratio will tend to a constant with decreasing number of samples. Note that the number of samples decreases from right to left in Figure 3.

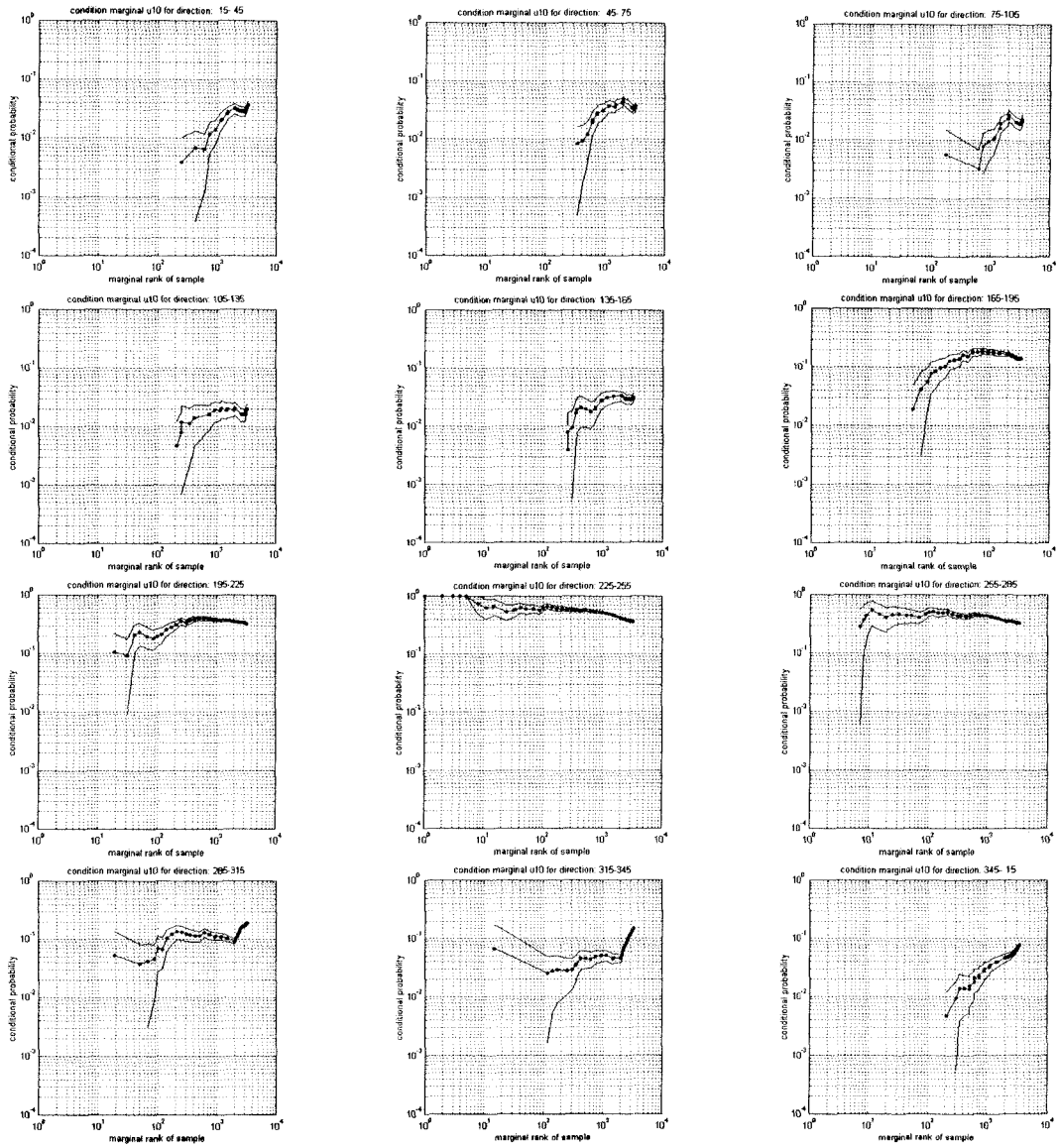

Figure 3 Ratio's of directional to omnidirectional exceedance frequency for wind speed derived from the data as a function of the number of samples (first row: sectors 1-3, second row: sectors 4-6, etc.)

The conclusions drawn from figure 3 are summarised in the table below.

sector no.	1	2	3	4	5	6	7	8	9	10	11	12
wind direction	015-045	045-075	075-105	105-135	135-165	165-195	195-225	225-255	255-285	285-315	315-345	345-015
wind speed	N	N	N	N	N	N	N	D!	D	D?	D	N
SWL	D	D?	N	N	N	N	N	N	N?	D!	D	D
surge	N?	D?	N	N	N	N	N	N	D?	D	D!	D

D: dominant N: not dominant ?: not clear !: highest probability

Table 4 Dominant and non-dominant sectors as concluded from Figure 3 (for wind speed), Figure 6 (for SWL) and Figure 7 (for surge).

The result for sector 10 (285-315) was not entirely clear. Values corresponding to the highest samples in the plot indicate that this sector is not dominant, but this does not fit with the trend in the remaining data-set and moreover, is inconsistent with the sectors 9 and 11. At Vlissingen, a wind from sector 10 blows approximately parallel to the coastline, so it is suspected that the highest wind speeds measured in this sector were reduced by sheltering (see also Section 2.2).

The next analysis step was the estimation of Weibull distributions for each direction. It was decided to use for all sectors the same value of the shape parameter α as in the omnidirectional curve (see table 1). Values of the 10,000 year quantiles were taken from Rijkoort & Wieringa see Table 5 and Figure 5. Therefore, only the thresholds ω exceedance frequencies $\mu(\omega)$ of the thresholds were to be estimated; values of σ were matched to the given quantiles. Table 5 summarises the final values and Figure 4 shows the fit to the sample exceedance frequencies. The fit is not for all directions very close, but it should be remembered that the wind data of Vlissingen were not properly corrected (we just applied a crude overall reduction of the exceedance frequency), so this does not mean that something would be wrong with the estimates.

	1	2	3	4	5	6	7	8	9	10	11	12
σ [m/s]	2.97	3.14	3.03	2.81	2.91	3.09	4.17	4.51	5.16	5.32	4.26	3.41
ω [m/s]	11.40	11.75	10.90	11.15	11.75	15.95	17.25	19.75	18.75	15.75	12.95	11.90
μ(ω) [/yr]	0.488	0.538	0.575	0.375	0.450	0.413	0.463	0.388	0.513	0.413	0.450	0.463
q(4 ,000 yr) [m/s]	19.16	20.11	19.13	18.20	19.18	23.18	27.84	30.75	32.52	30.41	24.74	21.01
q(10,000 yr) [m/s]	20.00	21.00	20.00	19.00	20.00	24.00	29.00	32.00	34.00	32.00	26.00	22.00

Table 5 Weibull parameters of the directional wind speed marginals matched to 10,000 year quantiles from Rijkoort and Wieringa: scale parameter σ, threshold ω, its frequency of exceedance and the 4000 and 10,000 year quantiles.

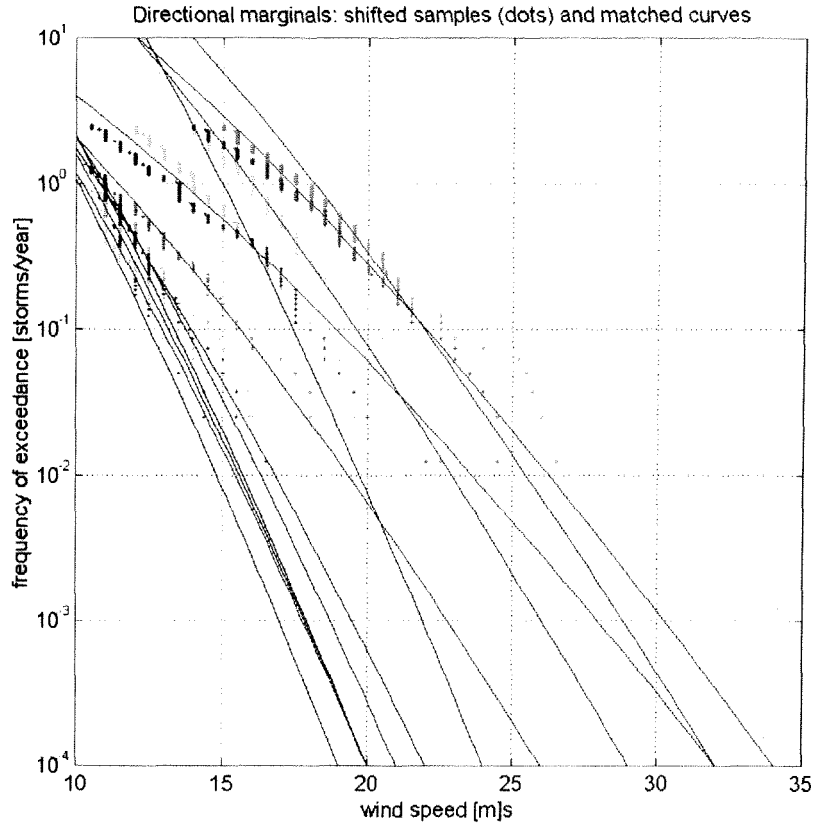

Figure 4 Estimates of the directional marginals of wind speed at Vlissingen (drawn) and sample exceedance frequencies reduced by factor of 5 (coloured dots). Colours correspond to wind directions; see Table 3.

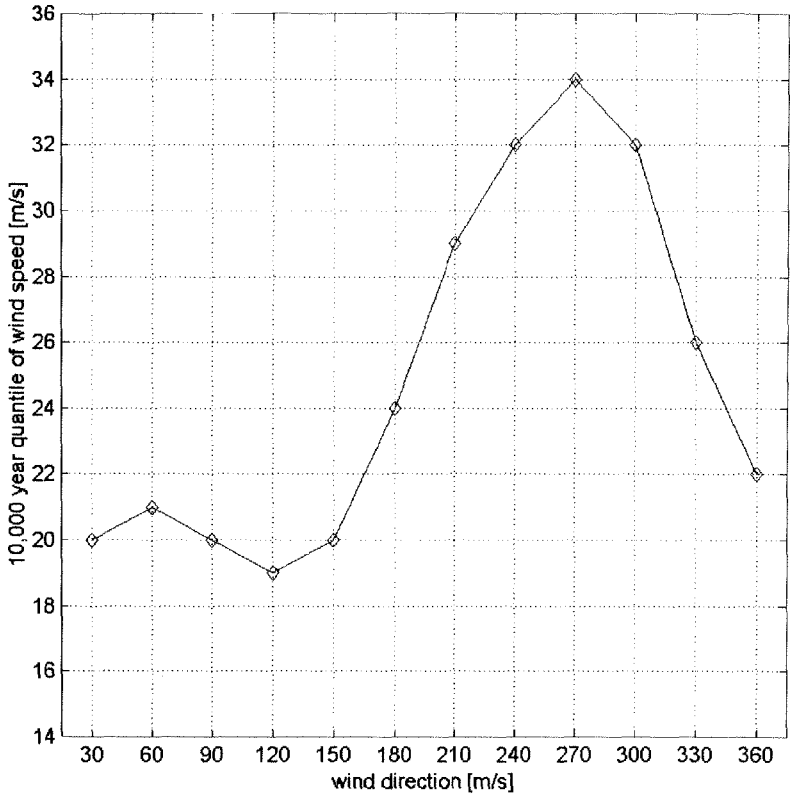

Figure 5 Conditional 10,000 year quantiles of wind speed in Vlissingen for the 12 wind direction sectors, based on Rijkoort & Wieringa.

2.4 Directional still water level marginals

The same analysis as described for wind speed was applied to still water level (SWL). Figure 6 shows again plots aimed to identify the directions which are dominant for SWL. For comparison, the sample plots were made for surge, which was simply the instantaneous difference of SWL and astronomical tide. In the outcomes for surge shown in Figure 7, less influence of the tide should be present, leading to less ambiguous results. The conclusions from these figures are collected in Table 4. It is clear that SWL and surge peak in more northerly directions than wind speed. The results for SWL and surge generally correspond, although not exactly.

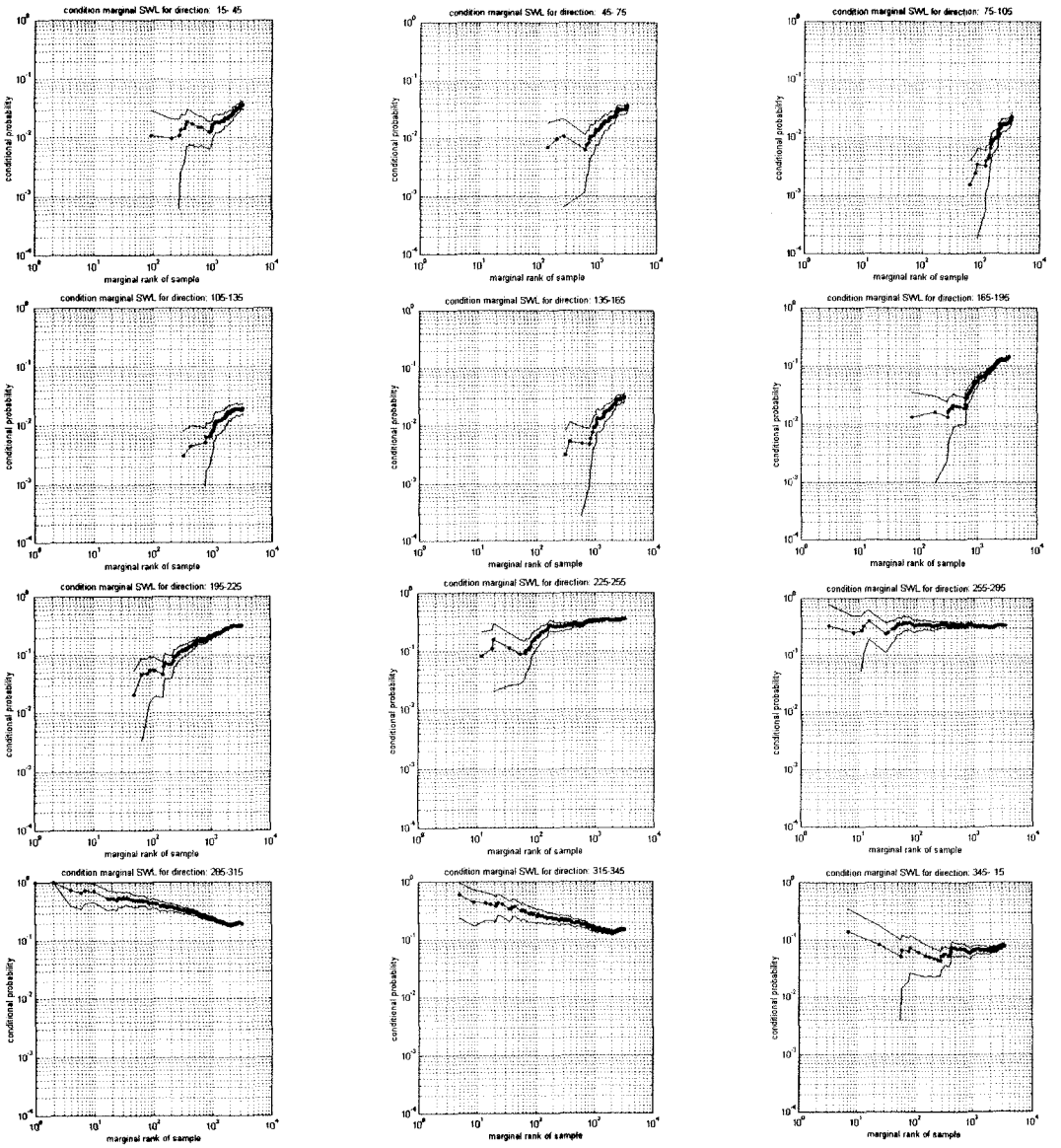

Figure 6 Ratio's of directional to omnidirectional exceedance frequency of SWL derived from the data as a function of the number of samples (first row: 1-3, second row: sectors 4-6, etc.).

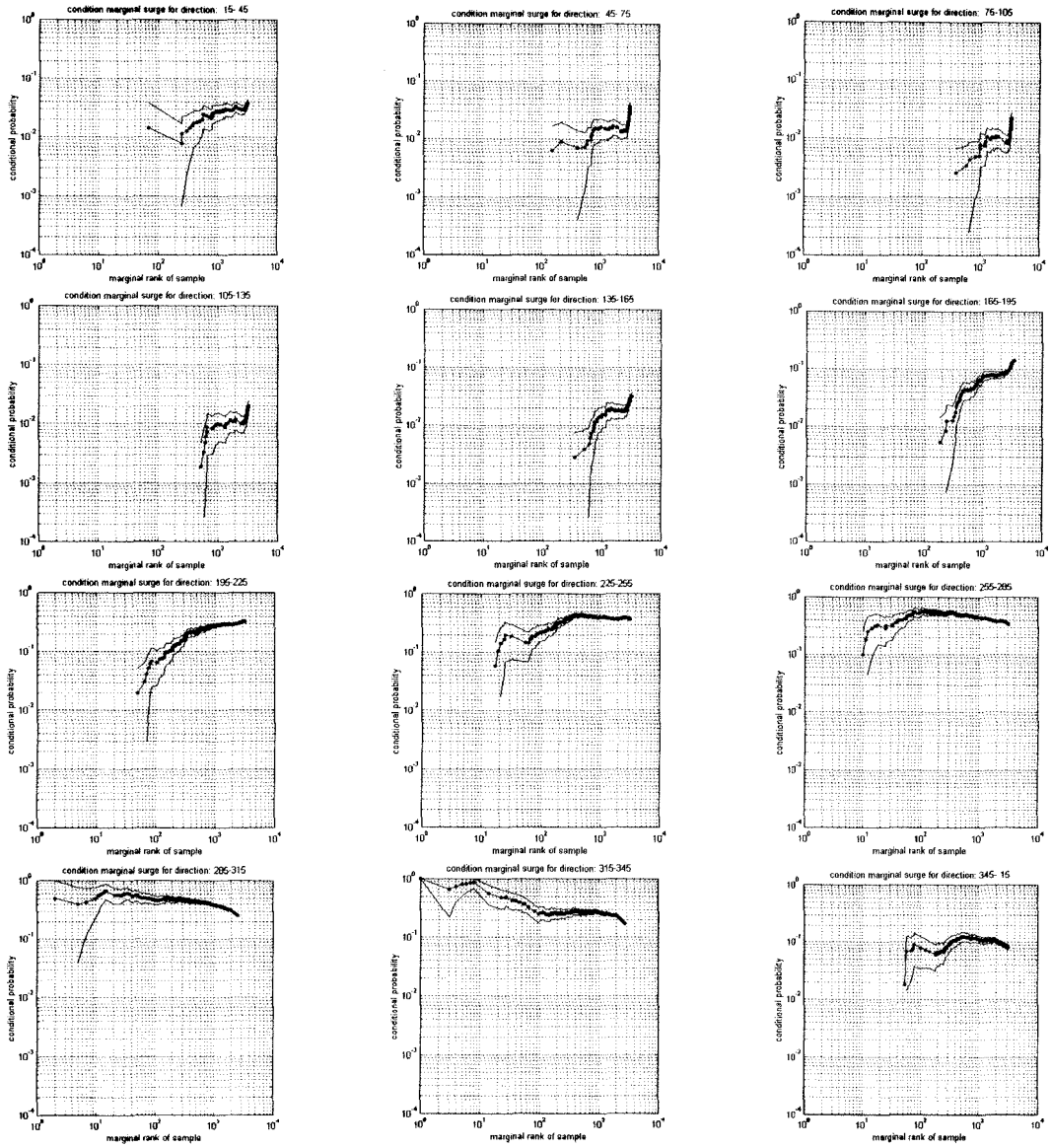

Figure 7 Ratio's of directional to omnidirectional exceedance frequency of surge level derived from the data as a function of the number of samples (first row: sectors 1-3, second row: sectors 4-6, etc.).

Again, the Weibull shape parameter for the directional marginals of SWL was fixed to the value of the omnidirectional marginal. Crude estimates of the scale parameter as a function of the number of samples are shown in Figure 8 below, Table 6 summarises the estimates, and Figure 9 shows the resulting directional marginals.

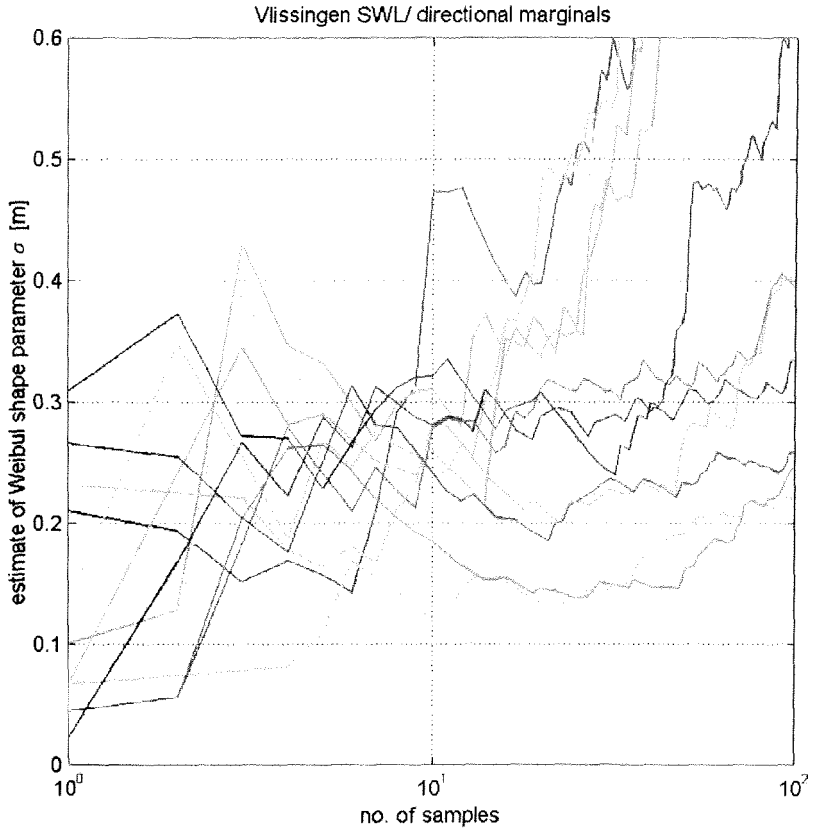

Figure 8 Estimate of scale parameter σ of the directional SWL marginals as a function of number of samples. Colours correspond to wind directions; see Table 3.

	1	2	3	4	5	6	7	8	9	10	11	12
σ [m]	0.27	0.27	0.27	0.22	0.22	0.22	0.17	0.17	0.22	0.27	0.27	0.27
ω [m]	2.4694	2.0848	1.5953	1.9275	1.9537	2.1198	2.6355	2.7754	2.8103	2.9589	2.9589	2.3995
μ(ω) [/yr]	0.3217	0.5429	0.4969	0.5070	0.6201	1.8759	1.2543	1.9530	2.1167	1.4734	0.9089	1.5033
q(4,000 yr) [m]	4.20	3.95	3.45	3.43	3.49	3.87	3.91	4.12	4.57	5.04	4.93	4.50

Table 6 Estimate of scale parameter σ, threshold ω, its frequency of exceedance and the 4000 year quantile of the directional SWL marginals.

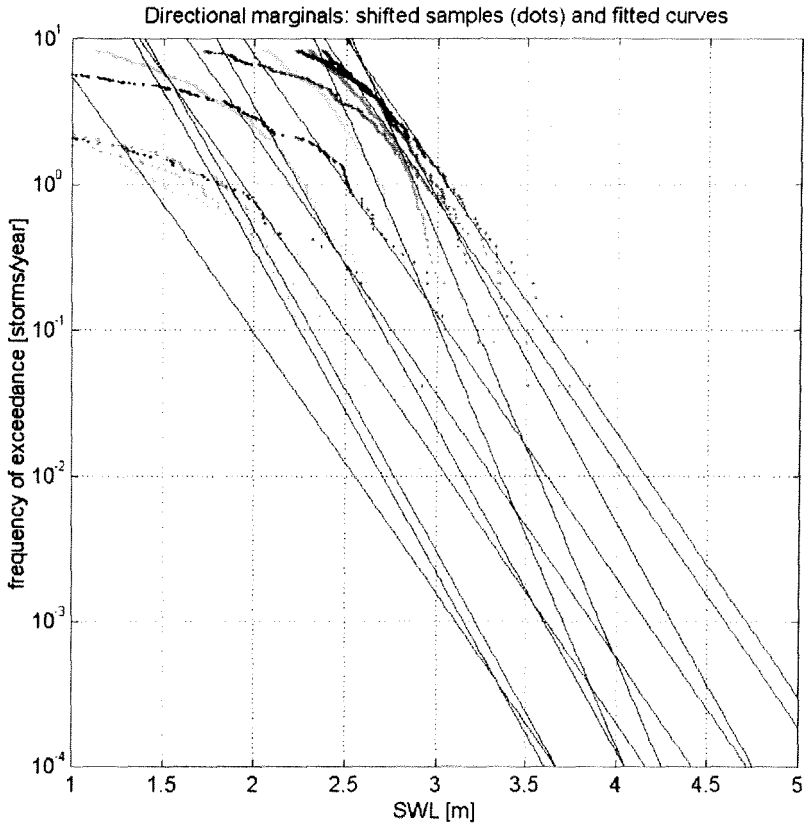

Figure 9 Estimates of the directional marginals of SWL at Vlissingen consistent with [Philippart et al., 1995] (corresponding with p= 0 m in eq. (1)). Colours correspond to wind directions; see Table 3. The final estimates have p=0.05 m so all quantiles are 0.05 m higher than those plotted.

The final estimates of conditional 10,000 year quantiles of SWL for the 12 wind direction sectors are given in figure 10 below; these include the offset p=0.05 m in eq. (1) (see Table 2).

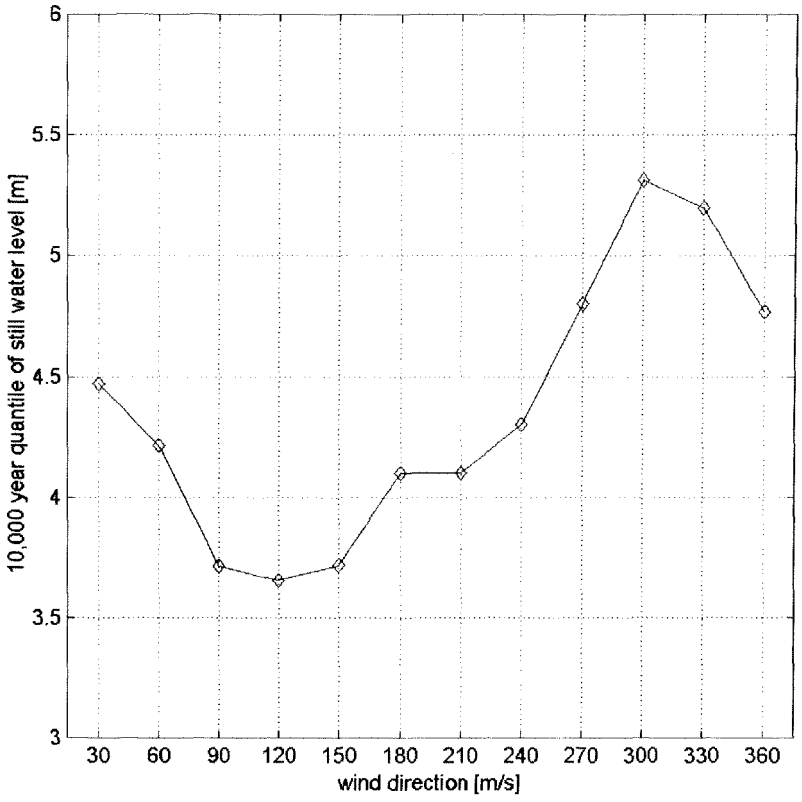

Figure 10 Estimated conditional 10,000 year quantiles of SWL in Vlissingen for the 12 wind direction sectors.

2.5 Dependence

In the method for approximating return periods of failure applied in this study (Chapter 4), wind speed and SWL at the storm maximum of SWL and coinciding with a wind direction in one of the sectors listed in Table 3 are assumed *asymptotically dependent*, see [De Valk et al., 1998]. Asymptotic dependence is a rather strong form of dependence. If asymptotically dependent variables have exponential marginal exceedance frequencies (or are each transformed such that their marginals become exponential), then the samples tend to be clustered around the main diagonal. This assumption has been verified for SWL and wind speed at SWL maxima by a check on asymptotic dependence carried out on directional storm maxima. The results are presented in Figure 11. If variables are asymptotically dependent, then the points in these figures should tend to a constant value toward the left (with fewer samples, only the highest are retained); this tendency is obscured by random fluctuations which increase in magnitude toward the left as well. The conclusion is that asymptotic dependence is likely to hold for the range of wind directions of 225°-345°. In the range of 165°-225°, the results indicate asymptotic independence. Outside these intervals, the situation is not clear. As generally wind directional in 225°-345° are expected to lead to the highest loads, the somewhat conservative assumption of asymptotic dependence of wind and SWL coinciding with SWL maxima for each of the 30° sectors may actually be quite reasonable in practice.

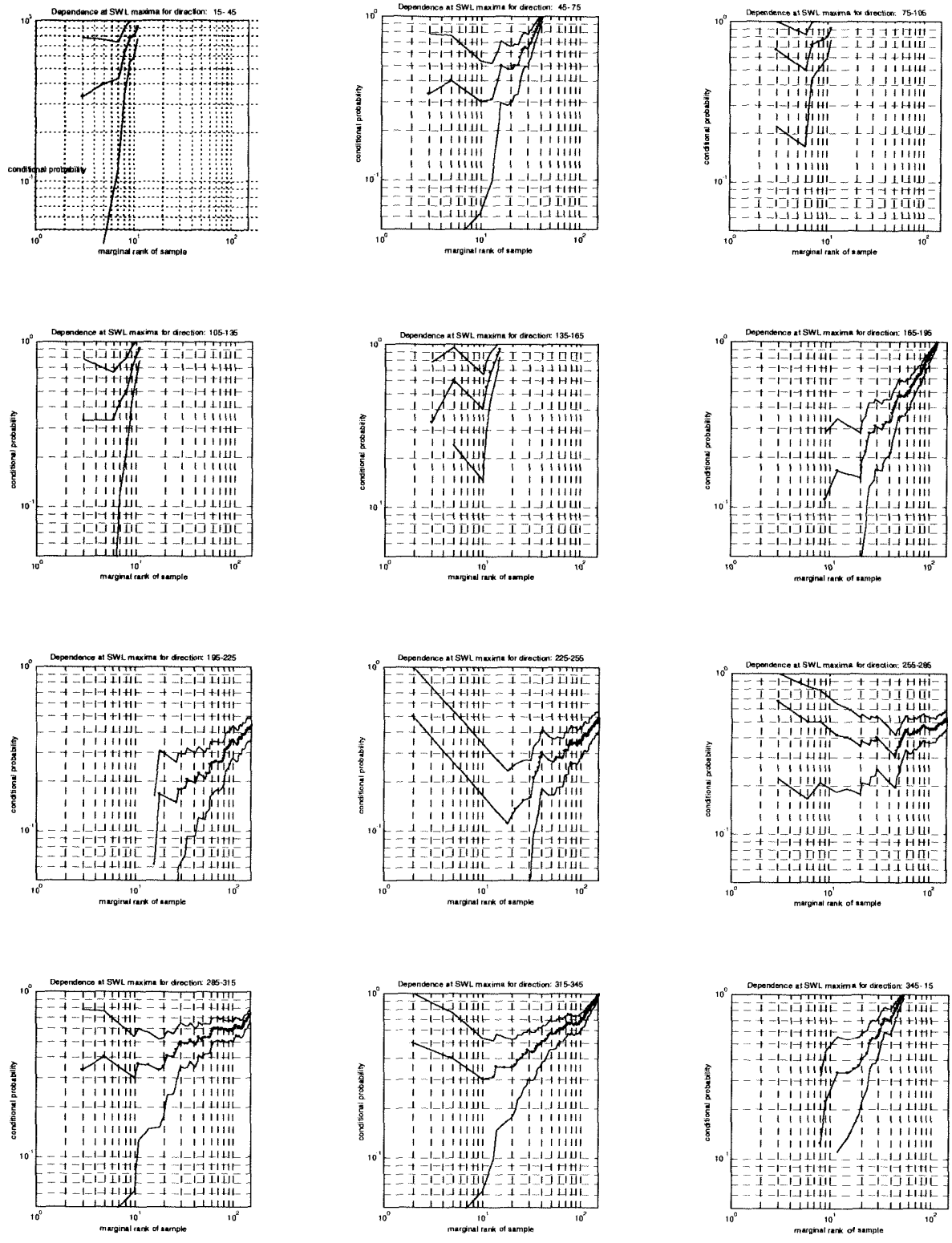

Figure 11 Check for asymptotic dependence of SWL and wind speed at SWL maxima carried out separately for twelve 30° sectors of wind direction.

This result applies only to the data coinciding with storm maxima of SWL. It can therefore be directly applied in our reliability analysis in Chapter 4, where for each storm we will only consider the wind and SWL which coincide with the storm maximum of SWL. However, the *marginals* of SWL at Vlissingen in Figure 9 were determined from *directional* storm maxima (taking the highest value of all samples in a storm which coincide with a particular wind direction). A directional storm maximum of SWL does not have to be the overall storm maximum of SWL. What we need is the frequency that the overall storm maximum of SWL exceeds a value and also coincides with a particular wind direction. This frequency is lower than the exceedance frequency of the directional storm maximum of SWL from Figure 9.

The same applies to wind speed marginals in Figure 4. In the reliability analysis, we need the frequency that the wind speed coinciding with the overall storm maximum of SWL exceeds a value and also coincides with a particular wind direction. This frequency is lower than the exceedance frequency of the directional storm maximum of wind speed in Figure 4.

The required reductions of marginals will be applied in a "non-parametric" manner as explained in [De Valk et al., 1998], assuming that the reduced exceedance frequencies are constant fractions of the exceedance frequencies of directional storm maxima. In words, this assumption means that for each sector, the directional storm maximum of SWL is also the overall storm maximum of SWL in a constant fraction of all storms, and that the directional storm maximum of wind speed coincides with the overall storm maximum of SWL in a constant fraction of all storms. It is a conservative assumption.

2.6 Conclusions

- Overall, the marginal fits seem to match the data rather well (after correcting the omni-directional frequencies, see Section 2). As a function of wind direction, all parameters vary smoothly for both wind speed and for SWL.
- The directional marginals for wind speed at Vlissingen may need to be improved upon later after applying appropriate corrections to the raw data which are dependent on wind direction. This is however not a task to be carried out in this study.
- Wind speed and SWL coinciding with SWL maxima appear to be asymptotically dependent for wind directions in 225°-345°.

3 Local models of waves, sea levels and dike failure

3.1 Description of the coastal sites

The six coastal sites labeled R1,...,R6 are shown in Figure 12. Their names are

R1 Citterpolder
R2 Borsselepolder
R3 Hansweert
R4 Margarethapolder
R5 Othenepolder
R6 Hoofdplaat

The foreshore elevation profiles can be find in the Alkyon report about wave modelling [Van Vledder, 1998, Figures 2.7-2.12]. In the wave model computations, the foreshores above 4 m - NAP were lowered by at most 0.5 m, which is also shown in the Alkyon report.

As seen in Figure 12 (Alkyon report), all sites are located at least 10 km from the inlet, so the direct effect of waves propagating from the North Sea is limited. It is expected that local generation of waves inside the estuary has greater impact than the propagation of waves from the North Sea.

Parameters of the six dike sections were estimated from elevation profiles shown in Figures 13-18; parameters estimated from these cross-sections are listed in the accompanying tables. In some cases, the values given are rather arbitrary as the profiles deviate considerably from the standard shape of a dike with two straight slopes separated by a berm. The toe levels listed are actually the elevations of the output points of the 1-D SWAN wave model used to predict wave conditions near the structure. The toe level is not used in the formulations for the failure mechanisms. In one case (section R2), the toe level listed is far below what appears to be the toe in the profile data. The latter have been altered by Alkyon to resolve inconsistency with the foreshore height data. The shore and dike profiles of R2 may need to be re-examined.

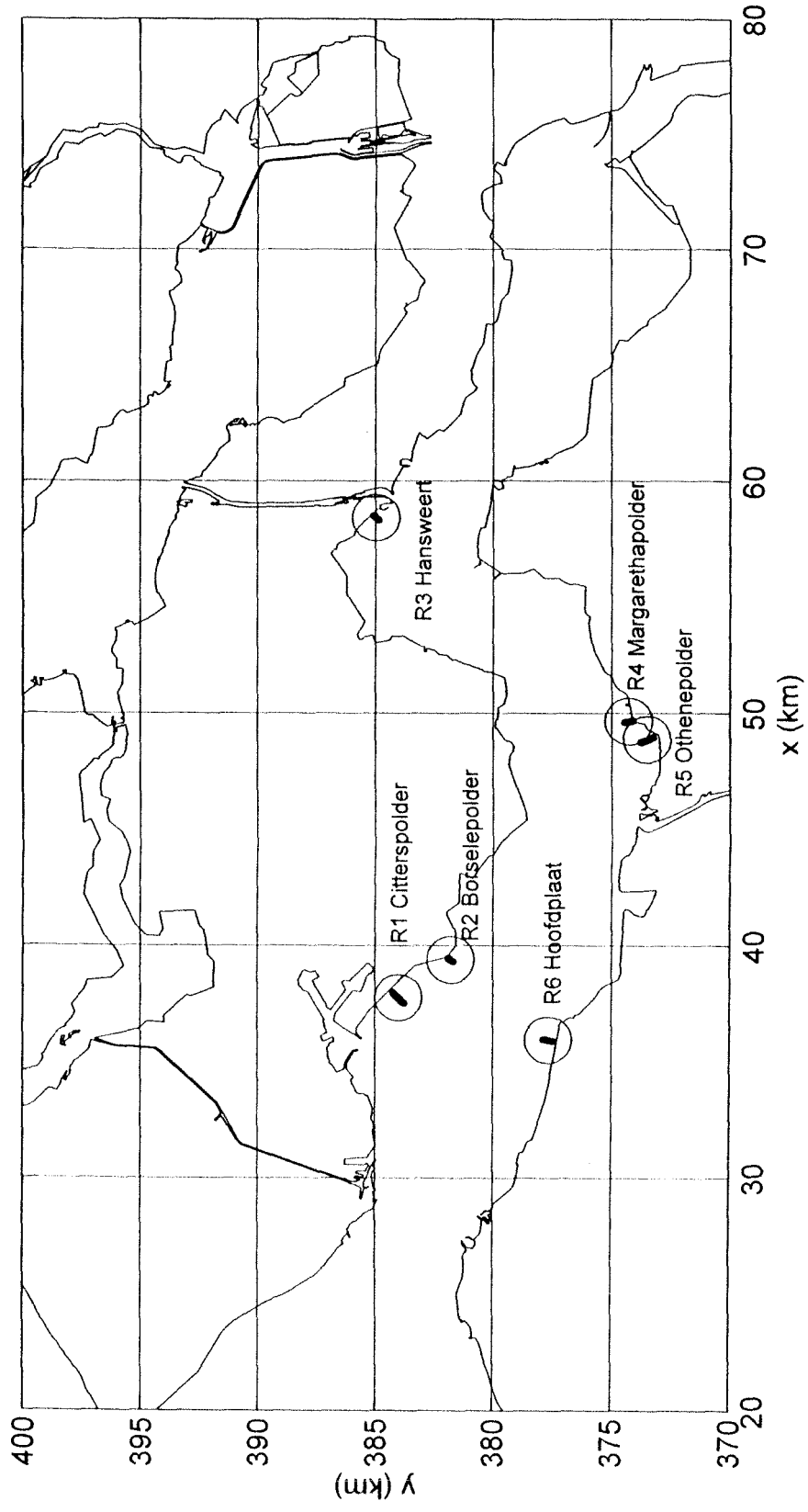

Figure 12 Westerschelde estuary and locations of dike sections (Alkyon report A240).

Citterspolder	Section R1	
Seaward normal	224	degrees (nautical)
Slope roughness	1	
Toe level	0.99	m +NAP
Berm level	2.38	m +NAP
Crest level	4.26	m +NAP
Berm width	13.42	m
Lower slope	0.102	
Upper slope	0.101	
Berm slope	0.007	

Table 7 Dike geometry Citterspolder.

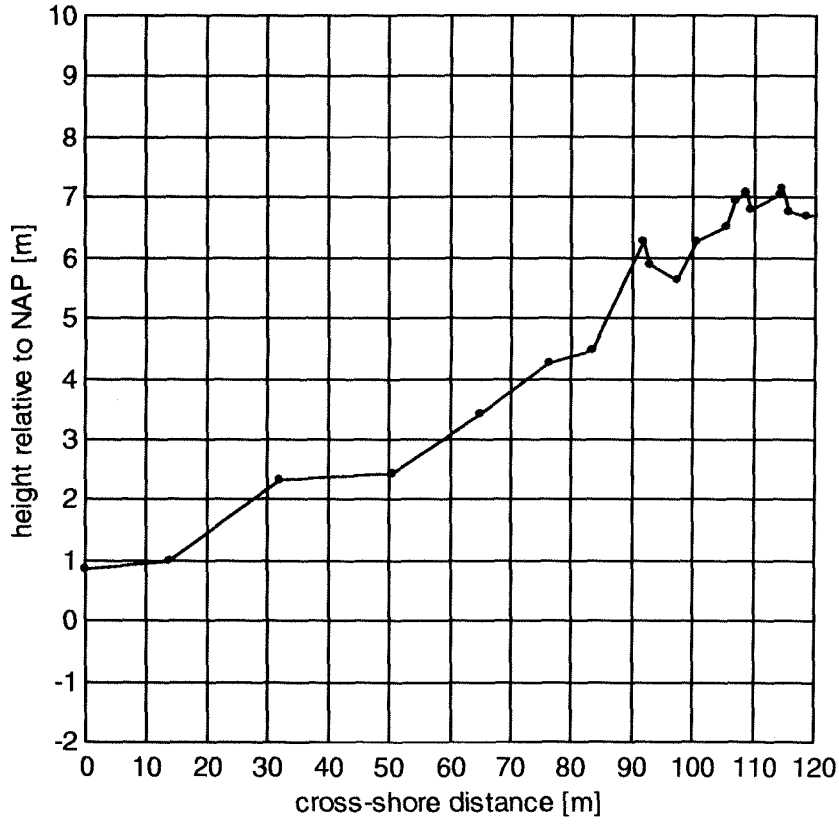

Figure 13 Profile of section R1 (Citterspolder).

Remark: the profile in Figure 13 is actually of a harbour breakwater and not of the dike of the Citterpolder. Sand dunes are present on the top. Awaiting the real dike profile of Citterpolder, the profile of Figure 13 was used temporarily in the load model for this location but it will need to be replaced.

Borsselepolder	Section R2	
Seaward normal	217	degrees (nautical)
Slope roughness	1	
Toe level	-1.97	m +NAP
Berm level	5.60	m +NAP
Crest level	8.66	m +NAP
Berm width	4.77	m
Lower slope	0.248	
Upper slope	0.570	
Berm slope	0.116	

Table 8 Dike geometry Borsselepolder.

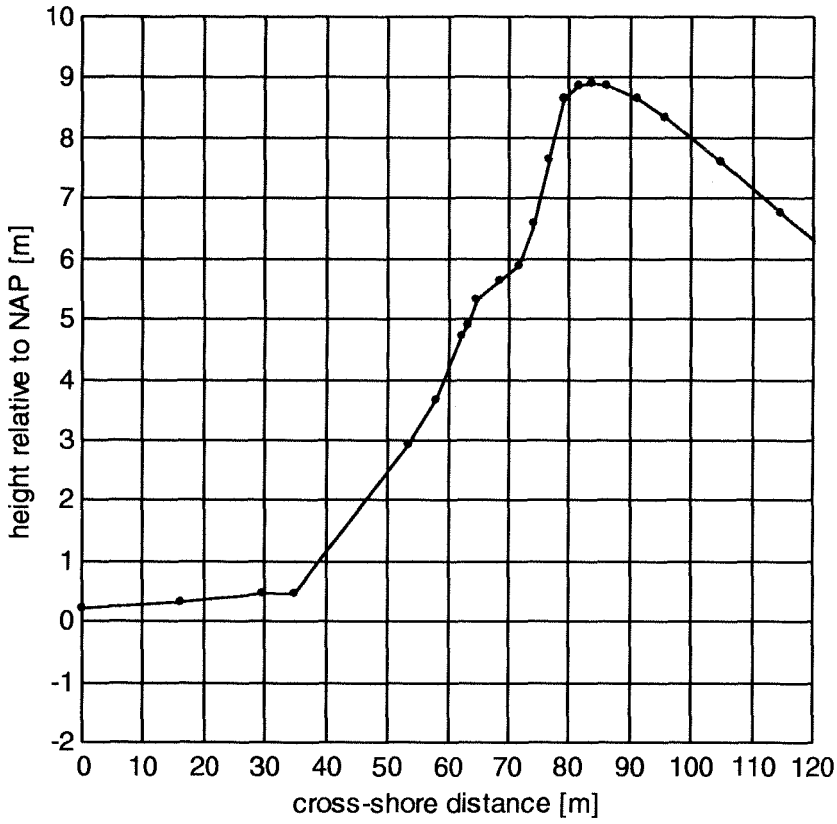

Figure 14 Profile of section R2 (Borsselespolder).

Remark: the profile near the toe of the dike differs from that drawn in Alkyon's report A240 on the wave model computations [Van Vledder, 1998; Figure 2.14]. The plot shown here is based on the original file Borsdp1t.asc. It has been modified later by Alkyon to match the foreshore profile. Table 8 corresponds to the modified profile.

Hansweert	Section R3	
Seaward normal	217	degrees (nautical)
Slope roughness	1	
Toe level	-1.23	m +NAP
Berm level	6.18	m +NAP
Crest level	8.33	m +NAP
Berm width	5.95	m
Lower slope	0.335	
Upper slope	0.369	
Berm slope	0.079	

Table 9 Dike geometry Hansweert.

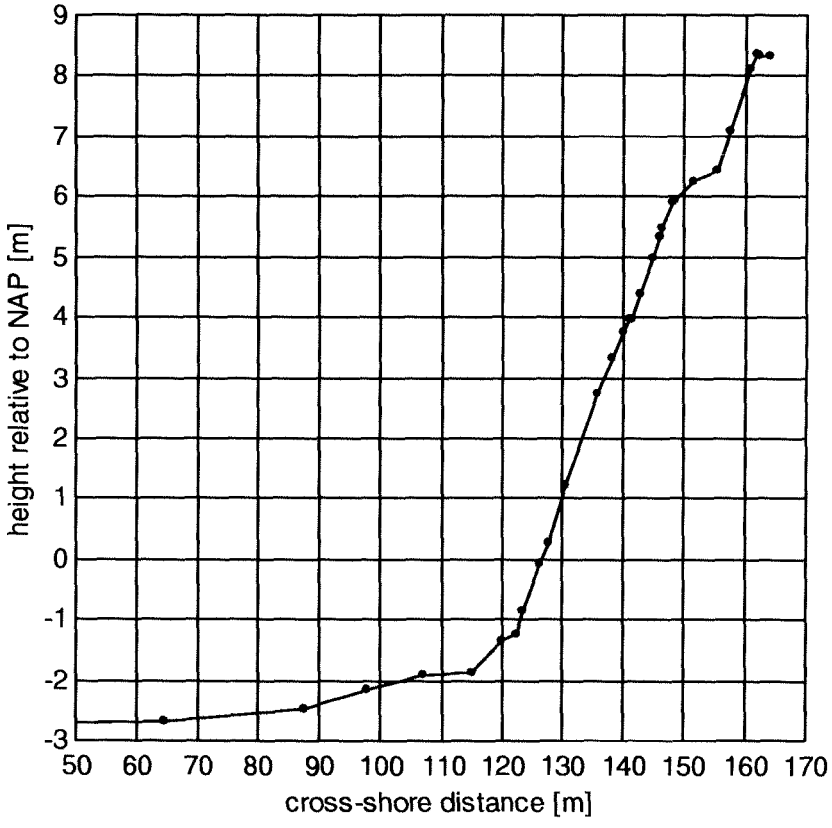

Figure 15 Profile of section R3 (Hansweert).

Margarethapolder	Section R4	
Seaward normal	349	degrees (nautical)
Slope roughness	1	
Toe level	-0.59	m +NAP
Berm level	5.96	m +NAP
Crest level	11.49	m +NAP
Berm width	8.80	m
Lower slope	0.271	
Upper slope	0.283	
Berm slope	0.083	

Table 10 Dike geometry Margarethapolder.

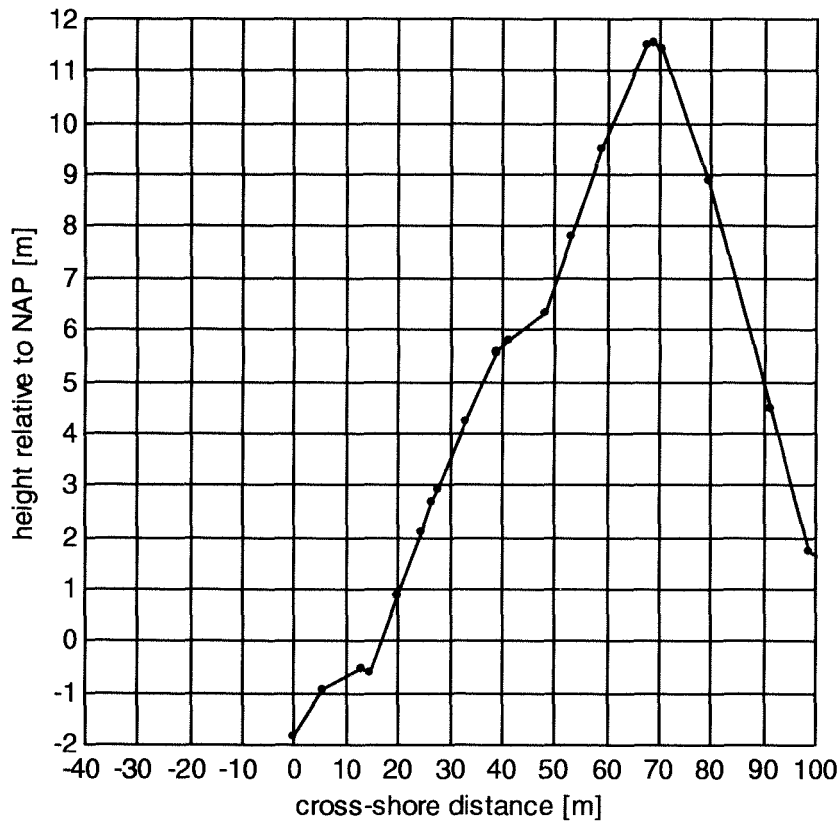

Figure 16 Profile of section R4 (Margarthapolder).

Othenepolder	Section R5	
Seaward normal	357	degrees (nautical)
Slope roughness	1	
Toe level	1.00	m +NAP
Berm level	5.61	m +NAP
Crest level	9.19	m +NAP
Berm width	7.57	m
Lower slope	0.291	
Upper slope	0.262	
Berm slope	0.046	

Table 11 Dike geometry Othenepolder.

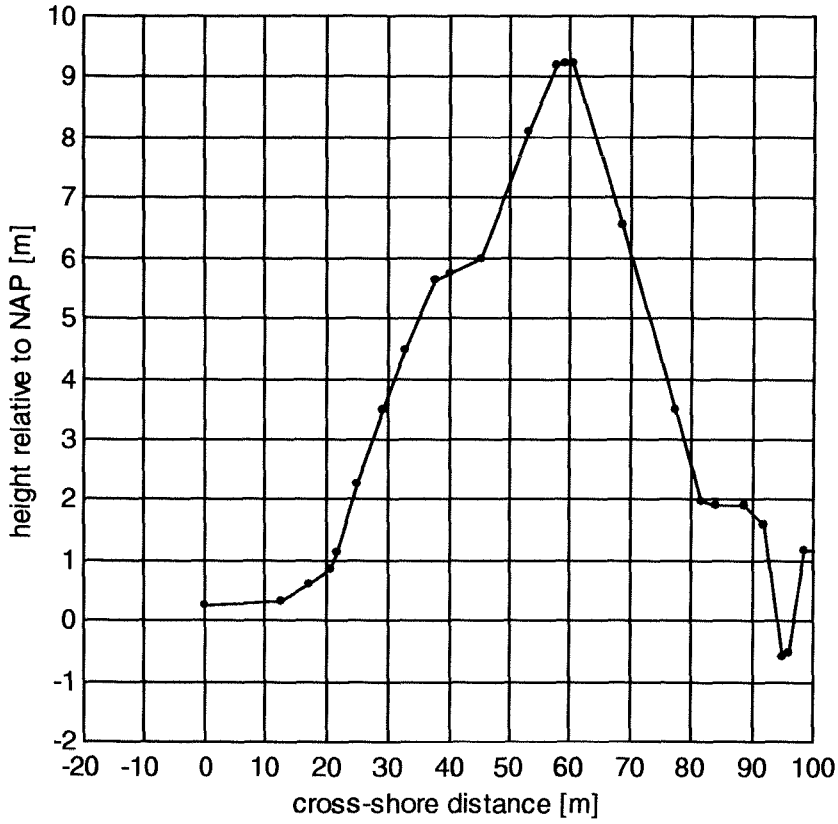

Figure 17 Profile of section R5 (Othenespolder).

Hoofdplaat	Section R6	
Seaward normal	11	degrees (nautical)
Slope roughness	1	
Toe level	1.37	m +NAP
Berm level	6.03	m +NAP
Crest level	10.66	m +NAP
Berm width	9.54	m
Lower slope	0.290	
Upper slope	0.328	
Berm slope	0.082	

Table 12 Dike geometry Hoofdplaat.

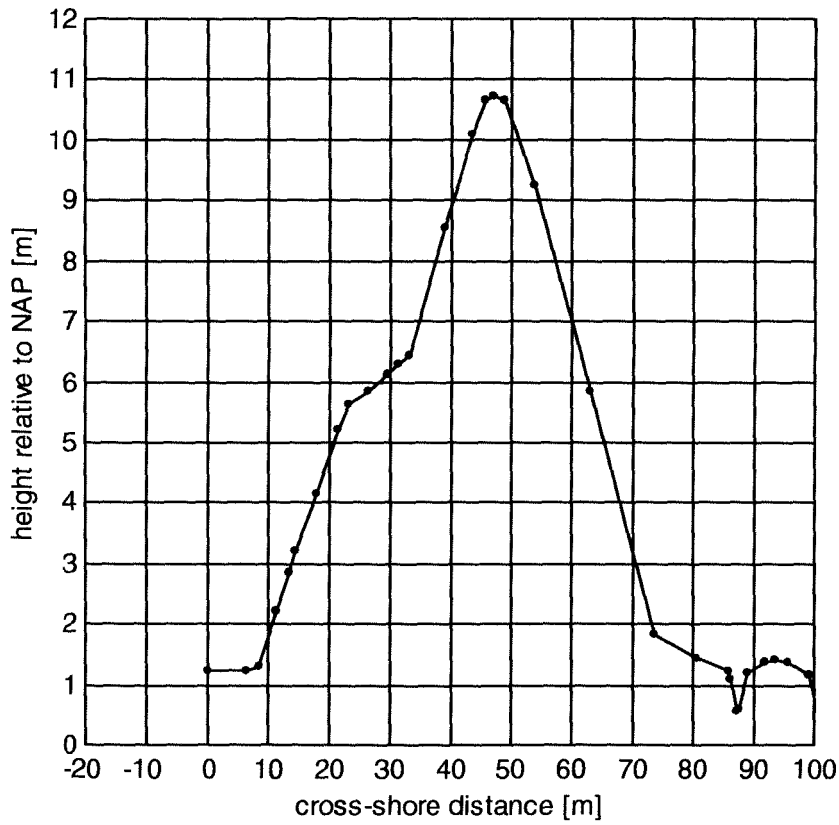

Figure 18 Profile of section R6 (Hoofdplaat).

3.2 Wave transformations and water level variation within the Westerschelde estuary

The input and output variables of the models in this study are

input variabeles		**output variables**	
SWL at *Vlissingen*	η	SWL *near structure*	η
windspeed at *Vlissingen*	u_{10}	significant wave height *near structure*	$H_{m,0}$
wind direction at *Vlissingen*		peak period *near structure*	T_p
		mean wave direction *near structure*	θ_0

For the wave model computations, we refer to Alkyon's report A240 [Van Vledder, 1998]. Model runs were performed assuming a flat SWL surface in the Westerschelde estuary, for the still water levels of 2, 4 and 6 m +NAP.

The wind speeds and directions applied in the runs are listed in the following table.

Direction (nautical)		**Wind speed 1**		**Wind speed 2**		**Wind speed 3**	
	Δ	**west [m/s]**	**east [m/s]**	**west [m/s]**	**east [m/s]**	**west [m/s]**	**east [m/s]**
030°	5	25	24	**20**	**19**	15	14
060°	5	26	25	**21**	**20**	16	15
090°	5	25	24	**20**	**19**	15	14
120°	5	24	23	**19**	**17**	14	12
150°	5	25	24	**20**	**19**	15	14
180°	5	29	28	**24**	**23**	19	18
210°	5	34	33	**29**	**28**	24	23
240°	5	37	36	**32**	**31**	27	26
270°	5	39	38	**34**	**33**	29	28
285°	5	38	37	**33**	**32**	28	27
300°	5	37	36	**32**	**31**	27	26
315°	5	34	33	**29**	**28**	24	23
330°	5	31	30	**26**	**25**	21	20
360°	5	27	26	**22**	**21**	17	16

Table 13a Wind speeds and directions applied in wave model computations. West/east is relative to the line Vlissingen-Breskens (continued on next page).

Direction (nautical)		Wind speed 4		Wind speed 5		Wind speed 6	
	Δ	west [m/s]	east [m/s]	west [m/s]	east [m/s]	west [m/s]	east [m/s]
030°	5						
060°	5						
090°	5						
120°	5						
150°	5						
180°	5	14	13				
210°	5	19	18	14	13		
240°	5	22	21	17	16		
270°	5	24	23	19	18	14	13
285°	5	23	22	18	17	13	12
300°	5	22	21	17	16		
315°	5	19	18	14	13		
330°	5	16	15				
360°	5						

Δ : Decrease in m/s between successive wind speed values.

Table 13b Wind speeds and directions applied in wave model computations. West/east is relative to the line Vlissingen-Breskens. (continuation of previous page)

Wind speed class 2 in this table corresponds to the same directional 4000 year quantiles for Vlissingen referred to in Chapter 1.

Variation of SWL within the estuary was derived directly from the SWL quantiles given in [Philippart et al., 1995]. This ignores the effect of e.g. wind direction or other variability, but it is simple. First, quantiles over a wide range of return periods were compared at the three locations Vlissingen, Terneuzen en Bath in the Westerschelde estuary. It was found that these quantiles were very well approximated by a single curve multiplied by a location-dependent constant. This reduced the problem to finding this constant for each of our six sites. At Vlissingen, Terneuzen en Bath, a relationship was derived between the sought constant and the 4000 year quantile. This relationship was combined with estimates of the 4000 year quantiles to determine the constants for the six sites. The estimated quantiles are the following.

Location		4000 year SWL quantile [m +NAP]
R1	Citterpolder	5.45
R2	Borsselepolder	5.50
R3	Hansweert	6.00
R4	Margarethapolder	5.80
R5	Othenepolder	5.80
R6	Hoofdplaat	5.47

Table 14 4000 year quantiles of SWL at six dike sections along the Westerschelde shore estimated from [Philippart et al., 1995].

Vlissingen	R1	R2	R3	R4	R5	R6
3.40	3.51	3.54	3.86	3.73	3.73	3.52
3.79	3.91	3.94	4.30	4.16	4.16	3.92
3.96	4.08	4.12	4.49	4.34	4.34	4.10
4.35	4.49	4.53	4.94	4.77	4.77	4.51
4.51	4.66	4.70	5.13	4.96	4.96	4.68
4.90	5.07	5.12	5.58	5.39	5.39	5.09
5.07	5.25	5.30	5.78	5.58	5.58	5.27
5.45	5.67	5.72	6.23	6.02	6.02	5.69
5.62	5.85	5.90	6.43	6.22	6.22	5.87
6.00	6.27	6.32	6.89	6.66	6.66	6.29

Table 15 SWL in metres +NAP at six dike sections along the Westerschelde shore as a function of SWL at Vlissingen

Table 15 gives SWL values at these sites as a function of SWL at Vlissingen. The table was linearly extrapolated down to -2 m NAP at Vlissingen assuming that everywhere, a zero SWL corresponds to a zero SWL at Vlissingen.

The SWL variability as estimated above was applied to correct the wave model computations, which were carried out assuming a flat SWL surface. It was assumed that nearshore wave conditions are only determined by the *local* SWL. This means that to obtain wave conditions at a dike section corresponding to a given SWL at Vlissingen, we first derive the local SWL interpolating/extrapolating Table 15, and then use this local SWL to interpolate/ extrapolate wave model outputs corresponding to the input SWL values of 2, 4 and 6 m +NAP with which model runs were made.

Interpolation and extrapolation of the wave model results was carried out in two steps. First, model output was extrapolated to lower wind speeds and water levels assuming that the logarithms of significant wave height and peak period are linear functions of SWL and the logarithm of wind speed. This avoids negative values. Extrapolation to higher wind speeds and water levels than applied in the model runs was done assuming that significant wave height and peak period are linear functions of SWL and wind speed. If outlyers result, these are normally less extreme than when extrapolating in terms of logarithms. The second step was to interpolate everything to a directionally independent set of values of wind speed, so the outputs are available on a regular grid of values of all input variables. To approximate model outputs for arbitrary input values, these regular data arrays can be processed rapidly by standard multilinear interpolation routines such as present in MATLAB 5.

Typical response surfaces of nearshore wave parameters as a function of wind speed and direction and for fixed SWL are shown for the location Borsselepolder in Figure 19. Part of the variation of the peak period with wind direction may be related to the ambiguity present in the definition of a peak period and its determination from a wave spectrum computed on a discrete spectral grid without assumptions on spectral shape. In view of the sensitivities associated with working with a peak period, there is a need for replacing peak period in the formulations for the various dike failure mechanisms by a sensible wave period measure based on spectral moments.

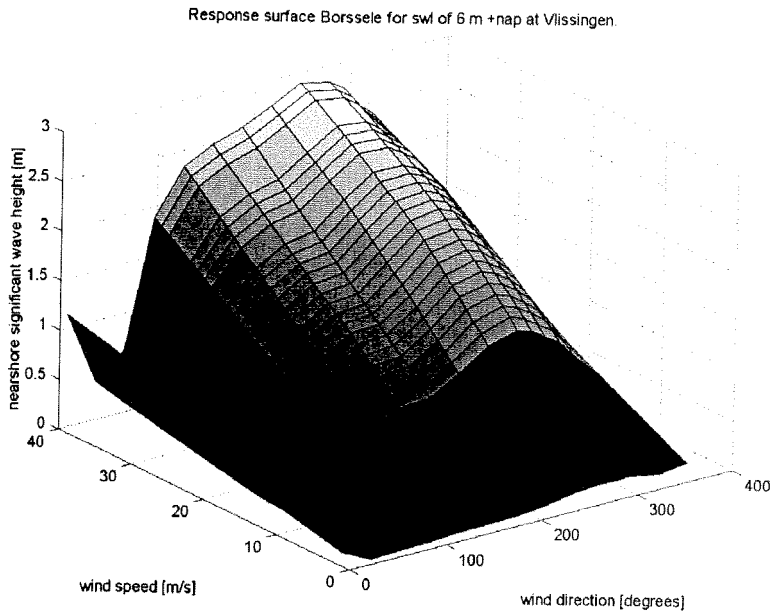
Response surface Borssele for swl of 6 m +nap at Vlissingen.
nearshore significant wave height [m]
3
2.5
2
1.5
1
0.5
0
40
30
20
10
0
wind speed [m/s]
0
100
200
300
400
wind direction [degrees]

(a)

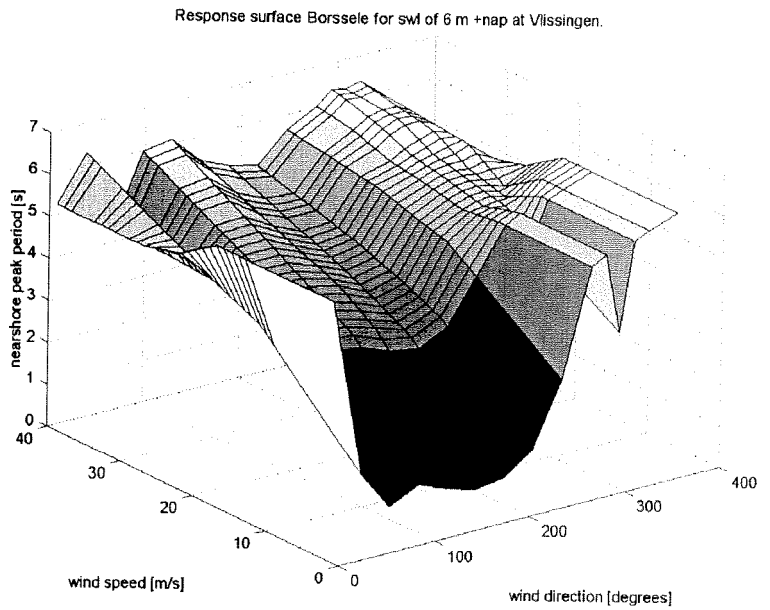
Response surface Borssele for swl of 6 m +nap at Vlissingen.
nearshore peak period [s]
7
6
5
4
3
2
1
0
40
30
20
10
0
wind speed [m/s]
0
100
200
300
400
wind direction [degrees]

(b)

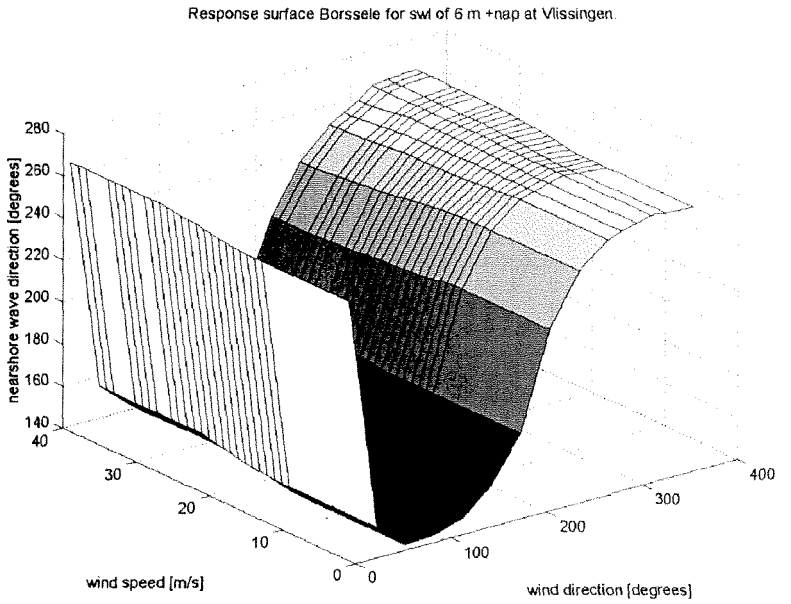

(c)

Figure 19 Response of significant wave height (a), peak period (b) and wave direction (c) at dike section Borsselepolder as a function of offshore wind speed and direction, all for a fixed SWL of 6 m +NAP at Vlissingen.

3.3 Failure mechanisms

Failure mechanisms considered in the present study are wave overtopping, wave run-up and a simple criterion for instability of a top layer of blocks of stone or concrete. Overtopping and run-up criteria are alternatives to account for the same failure mechanism, which is wave overtopping over the crest of the seawall or dike. Top layer instability is a different mechanism, so in estimating the return period of failure of a dike, it can be considered in conjunction with overtopping/run-up. Failure is expressed in terms of a reliability function z, which is negative if and only if the structure fails. The overall reliability function z is the minimum of reliability functions $z^1, z^2, \ldots$ for different failure mechanisms when these constitute alternative routes to failure:

$$z = \min(z^1, z^2, \ldots) \tag{3.1}$$

For wave overtopping, the reliability function used is

$$z^{\text{overtopping}} = q_c - q \tag{3.2}$$

with q the overtopping discharge per unit length of dike in litres/s/m, and q_c a critical value of q which cannot be exceeded without damage to the crest or rear slope. A typical value of q_c is 1 litre/s/m.

For wave run-up, the reliability function used is

$$z^{\text{run-up}} = h^{crest} - \eta - z_{2\%} \tag{3.3}$$

with h^{crest} the crest level relative to NAP, η the still water level SWL (possibly including infragravity waves) and $z_{2\%}$ the run-up height of the upper 2% of wave crests in excess of the SWL. Both q and $z_{2\%}$ are functions of SWL, significant wave height, peak wave period and mean wave direction at the toe of the dike.

Overtopping and run-up were implemented according to [TAW, 1998] based on [Van der Meer, 1997], with a few simplifying assumptions:

- the dike profile consists of a straight lower slope, a single straight berm and a straight upper slope leading to the crest;
- restrictions in the definitions of "slope", "berm" and "foreshore" in [TAW, 1998] are not checked, so e.g. anything called berm is treated as a berm;
- the surface roughness is supposed to be uniform along the profile and can be specified as a single number.

For instability of a top layer consisting of pitched blocks of concrete or stone, the following reliability function is used:

$$z^{\text{toplayer}} = 1 - \frac{H_{m,0}/\Delta D}{p} \tag{3.4}$$

with $\Delta = (\rho_s - \rho)/\rho$, ρ the density of water, ρ_s the density of the block, D the width of the top layer, and p the critical value of $H_{m,0}/\Delta D$. This critical value is as given for "type 3b" in Delft Hydraulics report H3161, and separates the safe range of values of $H_{m,0}/\Delta D$ from the values for which it is not sure whether the top layer will remain intact. It is:

$$\begin{aligned} p &= 4.04\xi_{op}^{-1.014} && \text{for} \quad \xi_{op} \le 2 \\ p &= 11.0\xi_{op}^{-4} + 0.03\xi_{op} + 1.25 && \text{for} \quad \xi_{op} > 2 \end{aligned} \tag{3.5}$$

with ξ_{op} the breaker parameter, which is the tangent of the slope divided by the square root of

$$s_{op} = 2\pi H_{m,0}/gT_p^2 \tag{3.6}$$

4 Reliability analysis

To approximate the return periods of failure, a *semi-parametric* extreme value method was applied described in [De Valk et al., 1998]. Semi-parametric means that the estimate is based on

- Predetermined marginal return periods of load variables like SWL, wind speed and significant wave height;
- A limited number of simultaneous observations of these variables, as well as of wave and/or wind directions. Alternatively, Monte-Carlo simulations can be used instead of observations.

Purpose of the method is to estimate the probability (or frequency) of a rare event far beyond the range of observations. The method is based on multivariate extreme-value theory developed over the last 25 years; see [De Haan en Resnick, 1977; Resnick, 1987]. Marginals need to be determined only for those variables which satisfy that the rare event of failure can occur with high values of one or several of these variables.

For each of these variables $(u_1,..,u_m)$, samples are determined of the *return period of exceedance*, which for a particular sample is the length of the period covered by the measurements divided by the number of storms in which this sample has been exceeded. The value of the return period of exceedance measures how rare the sample value of a variable is.

A population of more extreme samples is then simulated by simply multiplying the return periods for all variables by the *same* factor ρ. Plotting the sample return periods logarithmically, this amounts to shifting the samples over the same distance $\log\rho$ along all axes simultaneously. Using the marginals, values of the variables $(u_1,..,u_m)$ corresponding to these shifted samples can be computed from the return periods of exceedance. Therefore we can also determine the fraction f_ρ of shifted samples causing failure of the structure. Choosing ρ such that $f_\rho > 0$, the probability that the structure fails in an arbitrary storm is approximated by

$$P[z(u_1,..,u_m) < 0] \approx f_\rho / \rho \tag{4.1}$$

The multiplication of the return periods of exceedance of all samples for all variables by the same factor ρ is actually only allowed in a special case, namely, when these variables are *asymptotically dependent* (se also Section 2.5). This means that when the values of their return periods are plotted on logarithmic scales, the sample points tend to lie in a band of more or less constant width.

When the marginals are exceedance frequencies, it is a simple matter to ensure that the outcome of (4.1) is not a probability but a frequency of failure (the reciprocal of the return period of failure). The factor ρ can be chosen such that a predetermined number of shifted samples ends up in the failure domain. An example of samples of return periods of exceedance before shifting (black) and after shifting (coloured) is shown in Figure 20 for a fictive dike section along the west coast of Holland (the Pettemer Zeewering with increased crest height). The return periods of exceedance shown in the plot are of SWL and offshore wave peak period. The purple curve is the *limit state* (boundary of the failure

domain) for a critical wave overtopping discharge of 1 litre/m/s expressed in terms of the return periods.

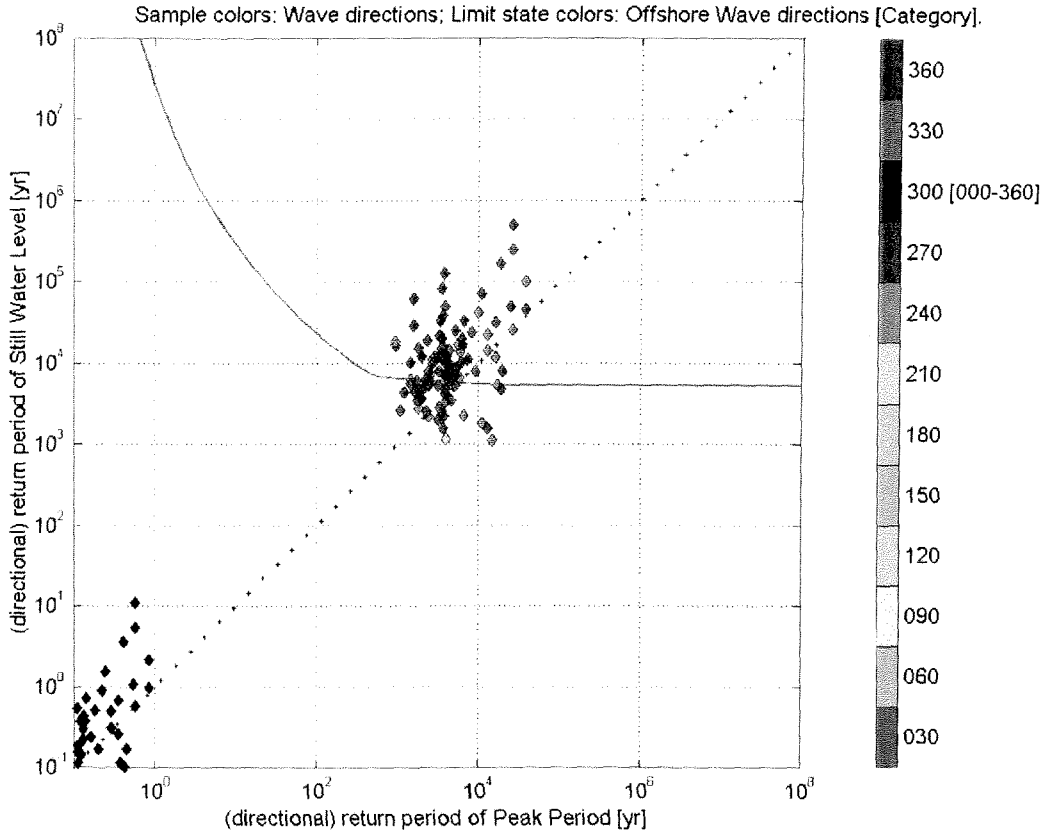

Figure 20 Example of measured (black) and shifted (coloured) return periods of SWL and offshore peak period plotted on logarithmic scales. The purple curve indicates the cross-section of the limit state surface in the plane of the variables displayed. Colours indicate offshore wave direction (see Table 3).

In the Westerschelde study, the input variables are SWL and wind (see also Section 2.4). We select only the values coinciding with the storm maxima of SWL. The method is slightly more complex than sketched above, as we consider the dependence between SWL and wind speed separately for each of the wind direction sectors in Table 3. We assume that at SWL maxima coinciding with a particular wind direction, SWL and wind speed are asymptotically dependent; this was verified in Section 2.4. The transformation of SWL and wind speed to their return periods is performed per sector of wind direction using the directional marginals from Chapter 1. However, the scaling of return periods by ρ is done simultaneously for all wind directions. For the Westerschelde dike section Borsselepolder and the failure mechanism wave overtopping (with a critical value of 1 litre/m/s), the figures 21-24 below show data samples, shifted samples, limit states, and contours of constant joint exceedance frequency in three different spaces:

- transformed offshore SWL and wind speed (having exponential marginals),
- offshore SWL and wind speed,
- nearshore variables: SWL, significant wave height, and wave peak period.

The computed return period of failure in this case is 5379 years. Generally, for all six locations, the results of the method look convincing enough. Estimates are reasonably stable as a function of the number of samples shifted into the failure region; see Figure 25. This is not trivial, and shows that the assumptions on mutual dependence of SWL and wind speed per wind direction sector are good enough, as they do apply for the most critical wind directions. Figure 26 finally summarises the offshore wind directions and nearshore wave directions of the most dangerous storms, which correspond to the shifted samples which lead to failure.

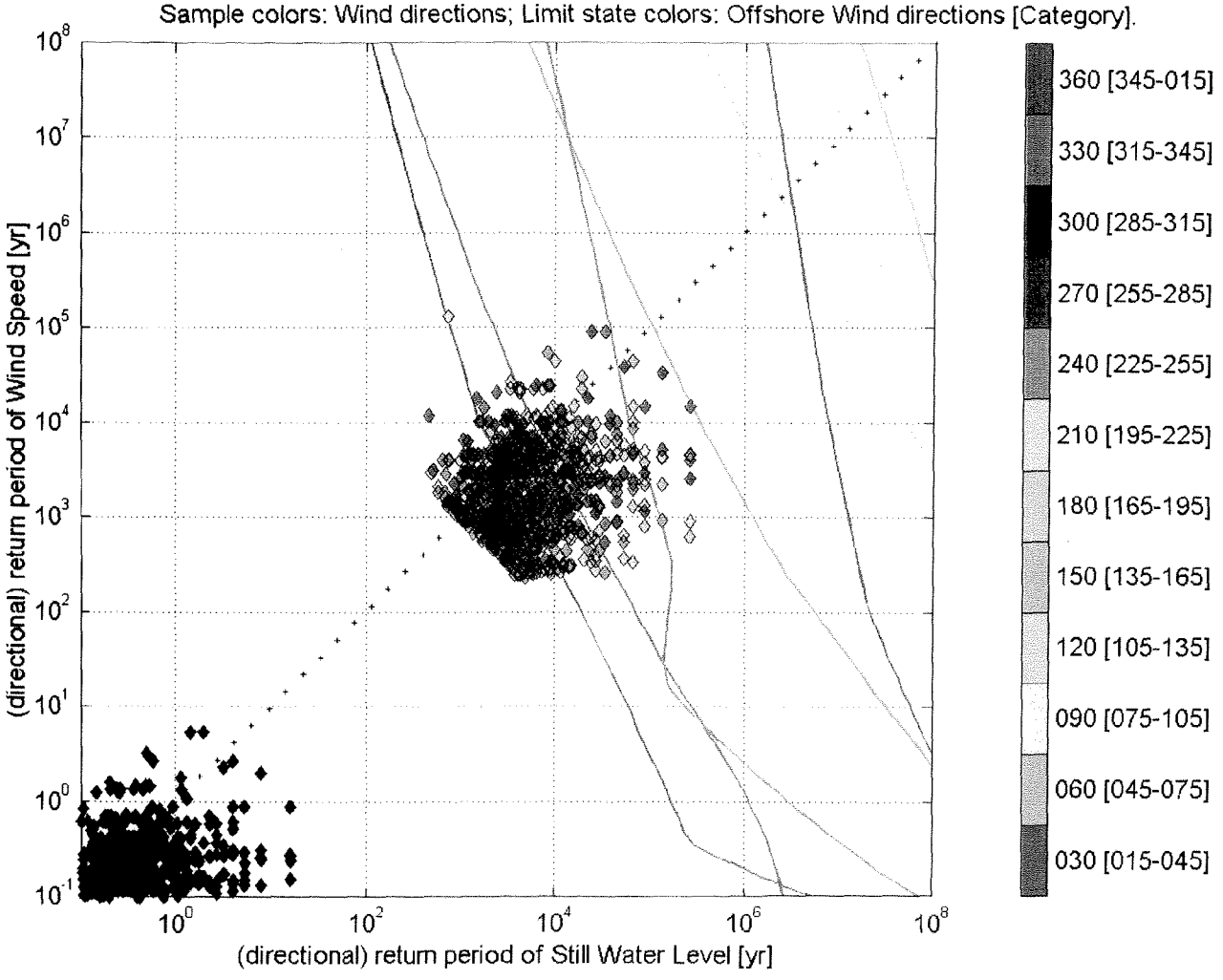

Figure 21 Overtopping Borsselepolder: samples (black) and shifted samples (coloured) of offshore SWL and wind speed transformed to variables having exponential marginals. The curves indicate limit state cross sections. Colours indicate wind direction.

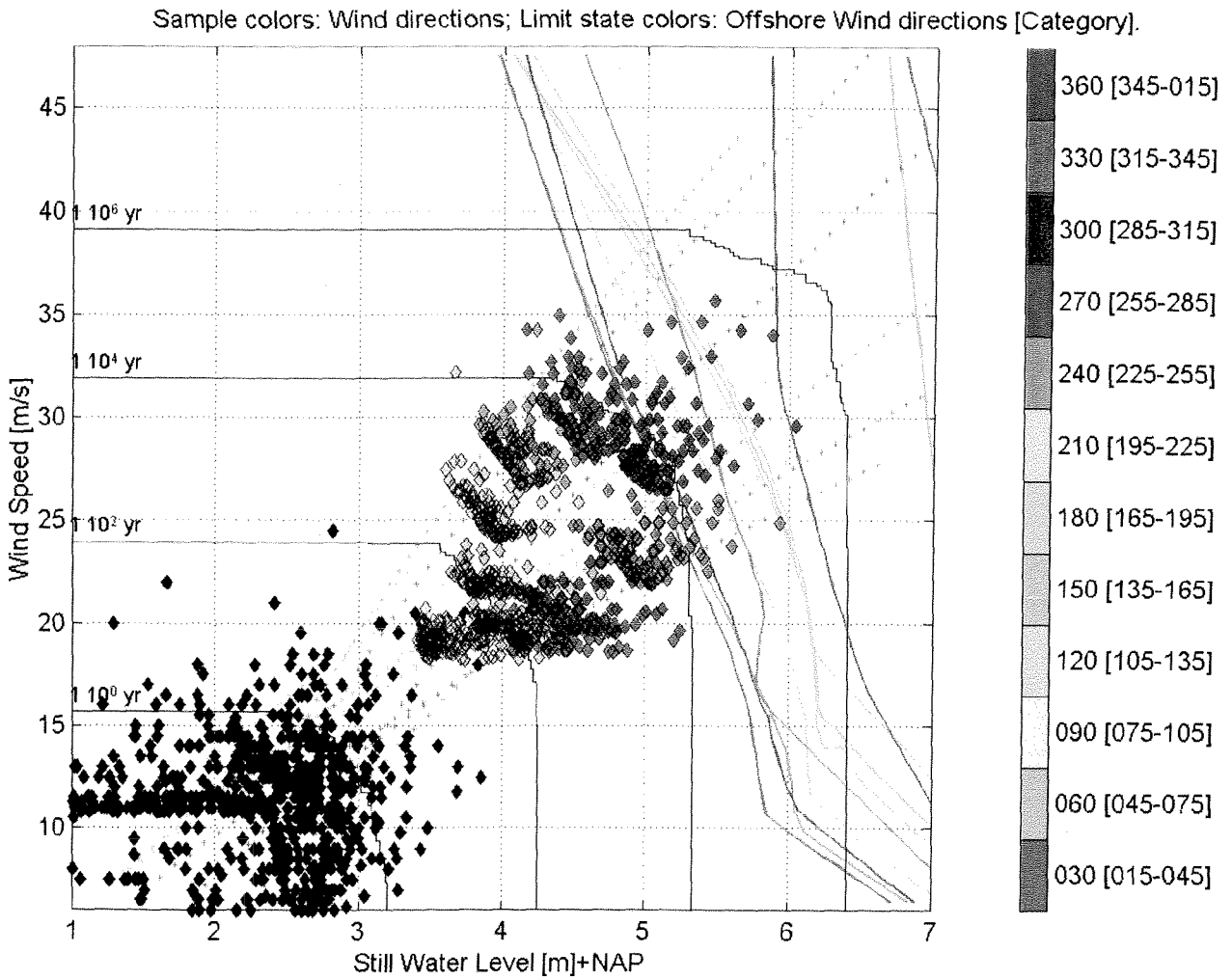

Figure 22 Overtopping Borsselepolder: samples (black) and shifted samples (coloured) of offshore SWL and wind speed. The curves indicate limit state cross sections Colours indicate wind direction.

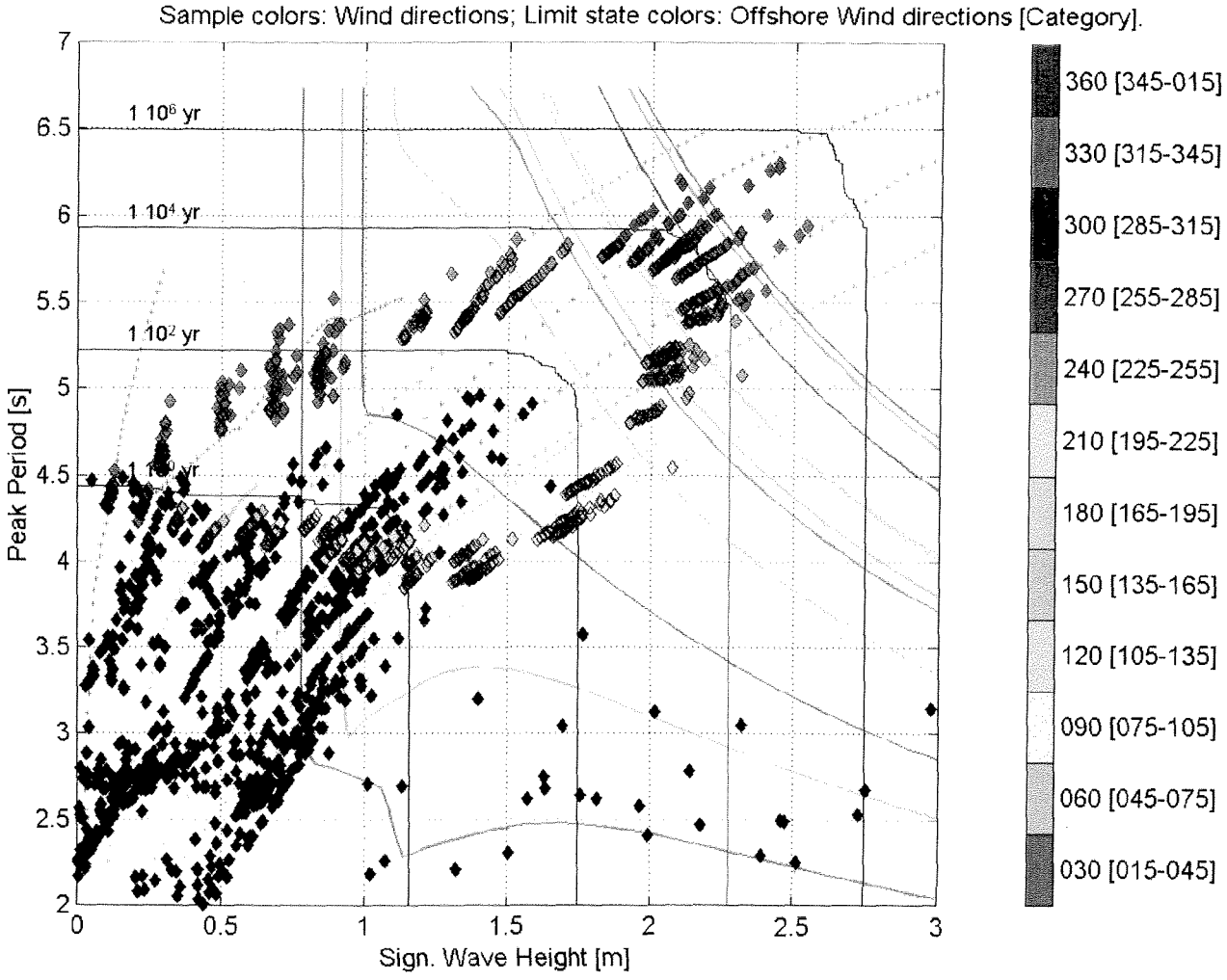

Figure 23 Overtopping Borsselepolder: samples (black) and shifted samples (coloured) of nearshore significant wave height and peak period. The curves indicate limit state cross sections computed using representative SWL and wave direction values for each wind direction. Colours indicate wind direction.

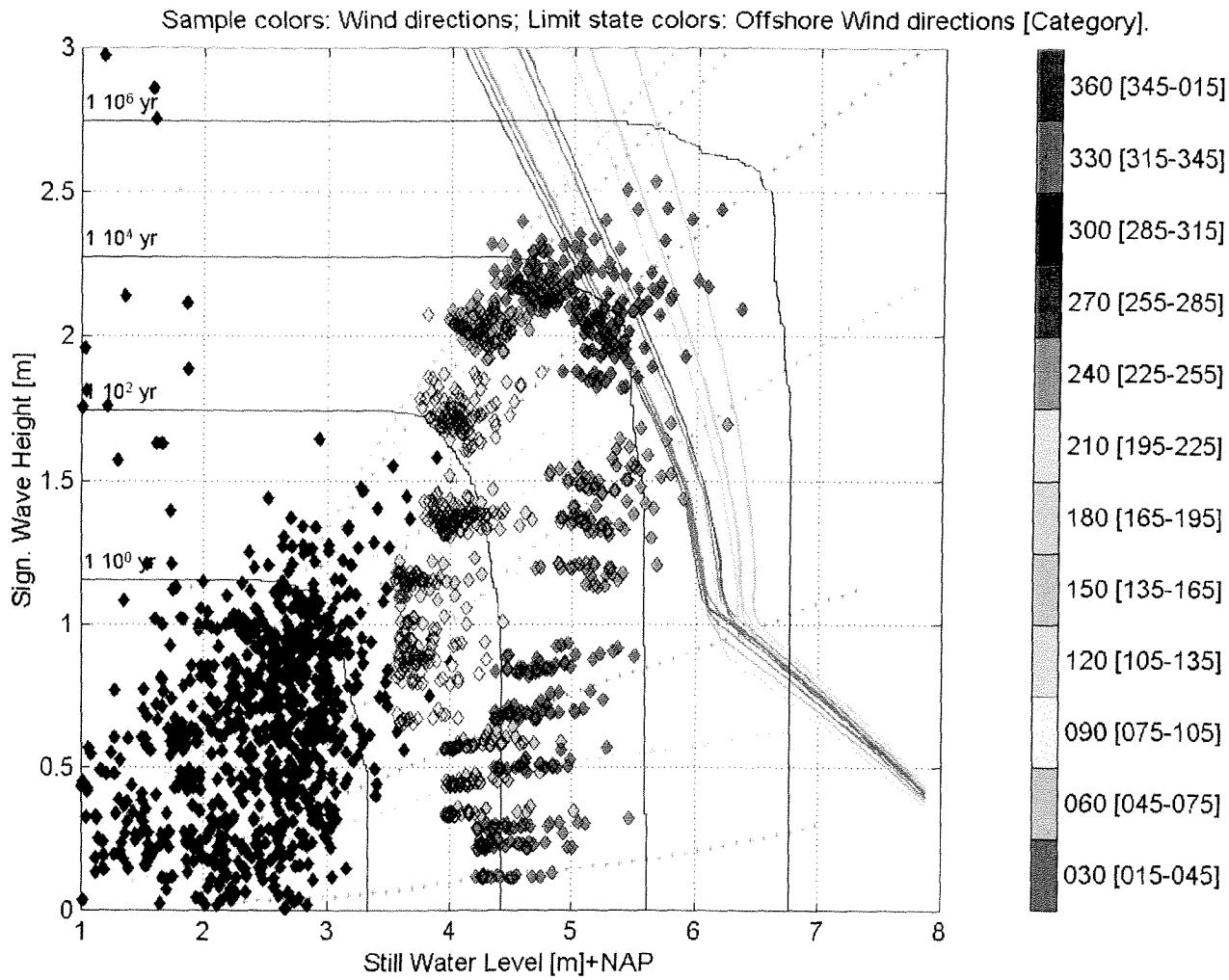

Figure 24 Overtopping Borsselepolder: samples (black) and shifted samples (coloured) of nearshore SWL and significant wave height. The curves indicate limit state cross sections computed using representative peak period and wave direction values for each wind direction. Colours indicate wind direction.

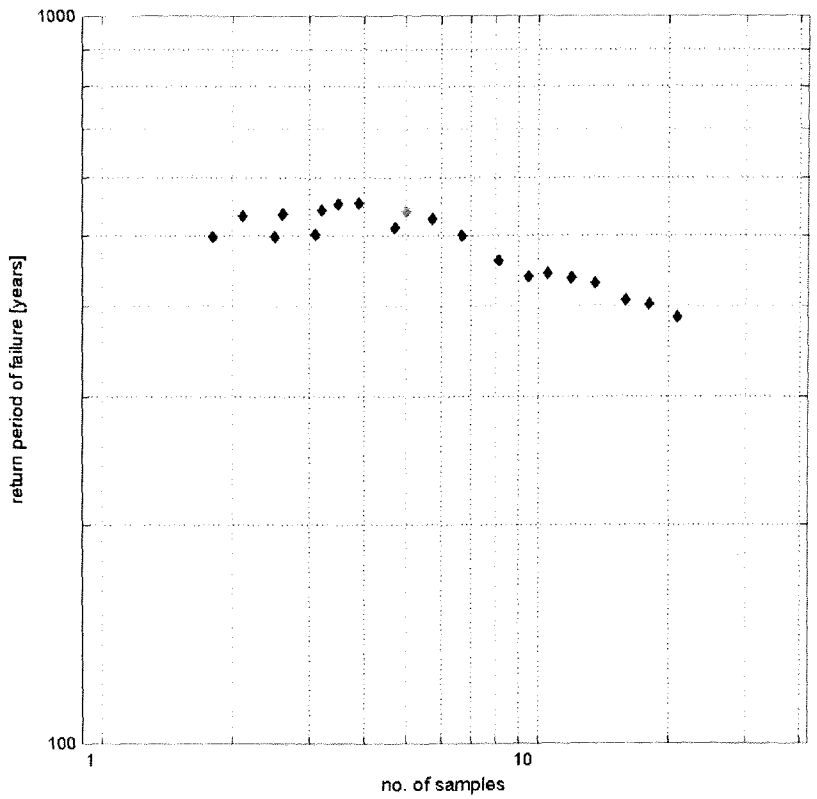

Figure 25 Overtopping Borsselepolder: estimate of return period of failure as a function of the number of samples shifted into the failure domain.

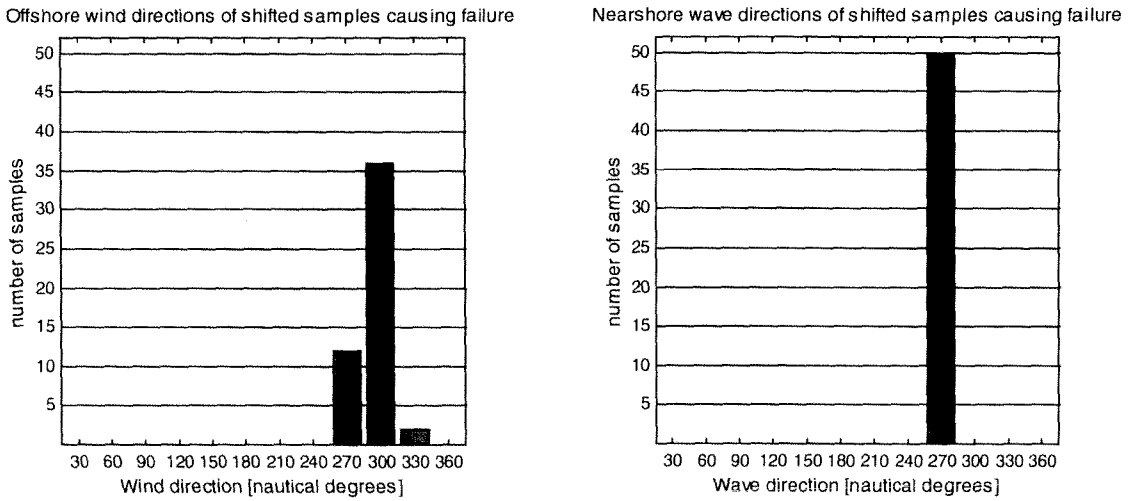

Figure 26 Overtopping Borsselepolder: histograms of offshore wind directions and nearshore wave directions of the most dangerous storms.

5 Accounting for uncertainties

5.1 Introduction

Uncertainty about the offshore joint distributions, the offshore-to-nearshore transformations and the behaviour of the coastal structure during storm conditions can be taken into account into the estimate of the return period of failure of a coastal structure. The frequency of failure is the expected number of storms per unit time causing failure, and the expectation should involve averaging over the possible values of uncertain variables. A local method to approximate this averaging was described in a previous report De Valk [1997]. This method is analogous to the widely used FORM (first order reliability method), see Hasofer and Lind [1974] or Ditlevsen & Madsen [1996].

The presentation of this method is extended here for the following reasons.

- To show that the local method allows us to partition the return period estimate into factors representing the estimate without uncertainty and the effects of different types of uncertainties. This provides valuable information about the relative importance of uncertainties such as marginal return periods, wave transformations, or behaviour of the structure. With this information, efforts to reduce the uncertainty (and thereby the total cost of building the structure) can be focused on the most important factors.
- The return period estimate *without* taking uncertainty into account is a function of the uncertain variables. The variance of the logarithm of this estimate is composed of contributions from different uncertain variables, each of which can be linked one-to-one to the factor by which the return period needs to be decreased to account for the uncertainty in this variable.

These findings can be translated into a format for presenting results to the user. Next, the feasibility of generalising the method to quantile estimates and automatic design of e.g. a crest level is investigated. Finally, a proposal is made for adjustments to the user interface of the reliability software to enable the user to switch uncertainties on and off in computations, and the technical realisation of adjusting the computational modules is examined.

5.2 Concepts and feasibility

5.2.1 Basics

Uncertainty about the values of strengths (or other variables such as marginal parameters, which we will simply refer to as strengths as well) is generally specified in terms of variances of deviations from a mean value; knowledge of the tail behaviour is normally not available. Also, in many cases tails of strengths are relatively short and therefore of little relevance.

A simple computational scheme to evaluate the frequency of failure for a structure with uncertain strengths can be obtained if the strengths are multivariate Gaussian. Assume that, at least locally, their distribution can be approximated by a multivariate Gaussian distribution, possibly after applying suitable marginal transformations to the strengths. Let the vector $\langle \mathbf{s} \rangle$ be the mean of the vector of strengths $\mathbf{s}$, and the matrix C its variance. Define

$$f(\mathbf{s}) = \log \mu[z(\mathbf{l},\mathbf{s}) < 0]. \tag{5.1}$$

the logarithm of the frequency of exceedance with the strengths $\mathbf{s}$ fixed. $f(\mathbf{s})$ depends only on the load statistics and can be approximated by the semi-parametric method. We want to compute the average ("$\mathbf{E}$" stands for expectation)

$$\mathbf{E}e^{f(\mathbf{s})} = \int_{s \in S} e^{f(\mathbf{s})} d F_s(\mathbf{s}) . \tag{5.2}$$

With F_s the distribution function of the strengths. Approximating f around a point $\mathbf{s}^0$ by a linear function

$$f(\mathbf{s}) \approx \mathbf{a}^T(\mathbf{s}-\mathbf{s}^0) + f(\mathbf{s}^0), \tag{5.3}$$

(with $\mathbf{a}^T$ an approximation of the local gradient of f) we obtain

$$\mu[z(\mathbf{l},\mathbf{s}) < 0] \approx e^{f(\mathbf{s}^0)} \mathbf{E} e^{\mathbf{a}^T(\mathbf{s}-\mathbf{s}^0)} = \mu[z(\mathbf{l},\mathbf{s}^0) < 0] e^{0.5\mathbf{a}^T C\mathbf{a} - \mathbf{a}^T(\mathbf{s}^0 - \langle \mathbf{s} \rangle)}. \tag{5.4}$$

The last identity in (5.4) can be proven by straightforwardly working out the details, or by noting that

$$\mathbf{E}e^{\mathbf{a}^T(\mathbf{s}-\langle \mathbf{s} \rangle)} = \chi(-i\mathbf{a}), \tag{5.5}$$

with χ the characteristic function of the random vector $\mathbf{s}$, and using the expression for the characteristic function of a Gaussian random vector; see *e.g.* [Itô, 1987]. (5.4) consists of a failure frequency at $\mathbf{s}^0$, multiplied by a correction factor which accounts for the uncertainty in the values of the strengths. Note that the failure frequency at the design point does not involve any approximation, whereas the correction factor is based on a linear approximation of f. Using an approximation of f in the correction factor is not unreasonable in view of the approximate nature of the distribution function of the strengths used.

5.2.2 Mean-value approximation

If we take $\mathbf{s}^0 = \langle \mathbf{s} \rangle$ in (5.4), the correction factor equals $\exp(\frac{1}{2}\mathbf{a}^T C\mathbf{a}) \geq 1$. This is a so called "mean-value" approximation. The approximation $\mathbf{a}^T$ of the local gradient of f can be determined by finite differences of f around $\langle \mathbf{s} \rangle$.

5.2.3 Local approximation

To improve this approximation, it is logical to choose $\mathbf{s}^0$ such that the correction factor is smaller in $\mathbf{s}^0$ than in $\langle \mathbf{s} \rangle$, so

$$|\tfrac{1}{2}\mathbf{a}^T C\mathbf{a} - \mathbf{a}^T(\mathbf{s}^0 - \langle \mathbf{s} \rangle)| \leq \tfrac{1}{2}\mathbf{a}^T C\mathbf{a} \tag{5.6}$$

The correction factor can be made equal to one by choosing a point $\mathbf{s}^0$ in which

$$\tfrac{1}{2}\mathbf{a}^T C\mathbf{a} = \mathbf{a}^T(\mathbf{s}^0 - \langle \mathbf{s} \rangle). \tag{5.7}$$

Moreover, besides satisfying (5.7), we like to choose the $\mathbf{s}^0$ with the highest probability density. If we choose $\mathbf{s}^0$ as the point where the function

$$(\mathbf{s}-\langle \mathbf{s} \rangle)^T C^{-1}(\mathbf{s}-\langle \mathbf{s} \rangle) - f(\mathbf{s}) \tag{5.8}$$

is minimal, then (5.7) is satisfied in $\mathbf{s}^0$. Moreover, the gradient of the logarithm of the probability density of $\mathbf{s}$ is orthogonal to the surface of constant f at $\mathbf{s}^0$. As a consequence, $\mathbf{s}^0$ is a local maximum of the density on a surface of constant f, with the value of f chosen to make the correction factor in (5.4) equal to one. This is completely analogous to FORM.

In general, strength variables are assumed mutually independent. If they are not, we can only say something about the importance of individual variables by decorrelating them. This is achieved by the following transformation:

$$\beta^0 = C^{-T/2}(\mathbf{s}^0 - \langle \mathbf{s} \rangle) \tag{5.9}$$

with $C^{1/2}$ a square root of C, so $C = C^{T/2}C^{1/2}$. Moreover, it is convenient to work with variables which have zero mean and unit variance, so the sensitivities of a function to each of these variables is a direct measure of the importance of the uncertainty in that variable. This normalisation is achieved by (5.9) as well. So because β_j^v has zero mean and unit variance,

$$\left|\partial f / \partial \beta_j^0\right|^2 \tag{5.10}$$

is to first order the contribution of uncertainty in β_j^0 to the variance σ_f^2 of $f(\mathbf{s}) = \log \mu[z(\mathbf{l},\mathbf{s}) < 0]$.

After minimising (5.8), we have

$$(\nabla_{s^0} f)^T = 2C^{-1}(\mathbf{s}^0 - \langle \mathbf{s} \rangle) \tag{5.11}$$

so with (5.9),

$$(\nabla_{\beta_0} f)^T = 2C^{-T/2}(\mathbf{s}^0 - \langle \mathbf{s} \rangle) = 2\beta^0 \tag{5.12}$$

For a single component β_j^0 of β_0, this implies

$$\left|\partial f / \partial \beta_j^0\right|^2 = 4\left|\beta_j^0\right|^2 \tag{5.13}$$

The left-hand side of (5.13) gives the contribution of β_j^0 to the variance σ_f^2 of f (see (5.10)). Expression (5.13) shows that it can be derived directly from the value of β_j^0 at the minimum of (5.8), so the variance contributions can be computed without the arbitrary choices one needs to make to approximate derivatives numerically. The total variance is the sum

$$\sigma_f^2 = 4\sum \left|\beta_j^0\right|^2 \tag{5.14}$$

The fraction of σ_f^2 related to β_j is given by

$$\frac{\left|\beta_j^0\right|^2}{\sum \left|\beta_i^0\right|^2} \tag{5.15}$$

To assess the relative contributions of different decorrelated strength variables to the frequency of failure, note that

$$\frac{\mu[z(\mathbf{l},\mathbf{s}) < 0]}{\mu[z(\mathbf{l},\langle \mathbf{s} \rangle) < 0]} = \frac{\mu[z(\mathbf{l},\mathbf{s}^0) < 0]}{\mu[z(\mathbf{l},\langle \mathbf{s} \rangle) < 0]} \approx e^{0.5\mathbf{a}^T C \mathbf{a}} \geq 1 \tag{5.16}$$

is the factor by which the frequency of failure is increased due to uncertainty in the strengths (see (5.4) and (5.7)). Note that (by (5.9))

$$C^{1/2}\mathbf{a} = (\nabla_{\beta_0} f)^T \tag{5.17}$$

so with (5.13),

$$\frac{\mu[z(\mathbf{l},\mathbf{s}) < 0]}{\mu[z(\mathbf{l},\langle \mathbf{s} \rangle) < 0]} \approx e^{2\Sigma\left|\beta_j^0\right|^2} = \prod e^{2\left|\beta_j^0\right|^2} \tag{5.18}$$

The uncertainty of each decorrelated strength variable β_j has increased the total frequency of failure by a factor

$$\exp(2\left|\beta_j^0\right|^2) \tag{5.19}$$

It is recommended to present these factors, as well as the relative variance contributions (5.15) in a table, as these are relevant figures to the user.

5.2.4 Computing the local approximation

Without considering uncertainties so with fixed strength $\mathbf{s}$, $\mu[z(\mathbf{l},\mathbf{s}) < 0]$ is computed as

$$\mu[z(\mathbf{l},\mathbf{s}) < 0] = e^{-\lambda} \tag{5.20}$$

To find λ, we iterate using a single sample $\mathbf{l}^{(m)}$ which has the m-th lowest value of the reliability function $z^{of,n}(\mathbf{l}+\mathbf{1}\lambda,\mathbf{s})$. After finding the value of λ for which $z^{of,n}(\mathbf{l}^{(m)}+\mathbf{1}\lambda,\mathbf{s}) = 0$, we check whether $z^{of,n}(\mathbf{l}^{(m)}+\mathbf{1}\lambda,\mathbf{s})$ is still the m-th lowest value. If so, the iteration is completed. If not, then the sample with the m-th lowest value of $z^{of,n}(\mathbf{l}+\mathbf{1}\lambda,\mathbf{s})$ is found, and the iteration for λ is repeated.

Within this process, we can in fact incorporate the search for $\mathbf{s}^0$ minimising (5.8). With the current sample $\mathbf{l}^{(m)}$, we minimise

$$(\mathbf{s}-\langle\mathbf{s}\rangle)^T C^{-1}(\mathbf{s}-\langle\mathbf{s}\rangle) + \lambda \tag{5.21a}$$

under the constraint

$$z^{of,n}(\mathbf{l}^{(m)}+\mathbf{1}\lambda,\mathbf{s}) = 0, \tag{5.21b}$$

or equivalently, minimise

$$\mathbf{x}^T\mathbf{x} + \lambda \tag{5.22a}$$

under the constraint

$$z^{of,n}(\mathbf{l}^{(m)}+\mathbf{1}\lambda,\langle\mathbf{s}\rangle + C^{T/2}\mathbf{x}) = 0). \tag{5.22b}$$

After finding a new $\mathbf{s}^0$ and λ, we check whether the current $\mathbf{l}^{(m)}$ should be replaced as above. If not, then the problem is solved, and the frequency of failure is $\exp(-\lambda)$. All iteration for $\mathbf{s}^0$ is done using only a single sample; only at the end of a cycle, at least m samples are used to check whether $\mathbf{l}^{(m)}$ should be replaced. In practice, the number of cycles is small. The added computational load required to take uncertainties into account is therefore comparable to FORM.

In tests carried out with this method in [De Valk, 1997], the value of λ which satisfies the constraint in (5.11) was solved for in an inner iteration loop, and a general descent method (BFGS) employing finite difference gradient approximations was applied to solve the resulting unconstrained minimisation problem for $\mathbf{s}^0$. This approach was satisfactory, and is recommended for implementation.

5.2.5 Estimating quantiles

Just as we can correct return period estimates to account for uncertainties, we can do the same with estimates of quantiles, which are values exceeded with a specified frequency or return period. A 10,000 years nearshore wave height quantile, for example, can be decreased as a result of uncertainties about offshore marginals or in the shallow-water wave transformations employed. An overtopping discharge quantile can be decreased also by the uncertainties associated with the overtopping discharge formulation which was determined from flume experiment data.

In the presence of uncertainty, we will define a quantile as the value of a variable which is exceeded with a specified expected frequency, the expectation being over all uncertain variables ("strengths") considered. Define for some variable u

$$f_u(\mathbf{s}) = \log \mu[u(\mathbf{l},\mathbf{s}) < 0]. \tag{5.23}$$

with the strengths $\mathbf{s}$ fixed. Then the quantile $q(\mu^0)$ of u exceeded with a frequency μ^0 is the value for which

$$\mu^0 = \mathbf{E}\, e^{f_{q-u}} \tag{5.24}$$

Just as in 5.2.1, it is approximated as

$$\mu^0 \approx \mu[u(\mathbf{l},\mathbf{s}^0) > q] e^{0.5\mathbf{a}^T C \mathbf{a} - \mathbf{a}^T(\mathbf{s}^0 - \langle \mathbf{s} \rangle)}. \tag{5.25a}$$

with

$$\mathbf{a}^T = \nabla_s f_{q-u}(\mathbf{s}_0) \tag{5.25b}$$

the local gradient of f_{q-u} in the point $\mathbf{s}^0$.

It is clear that whatever the method employed (setting $\mathbf{s}^0$ equal to $\langle \mathbf{s} \rangle$ as in the mean value approach, or taking $\mathbf{s}^0$ to minimise (5.8) with f_{q-u} replacing f), some degree of approximation is needed: we need to guess a value for q, then approximate the frequency of exceedance $\mu(q)$ of q, compare it with the specified frequency μ^0 and choose a new value for q, until $\mu(q) = \mu^0$. Taking uncertainty into account, this computation needs to be repeated for each variable u of interest. It is no longer possible to obtain quantiles of all variables of interest from the same computation as was the case without uncertainties.

In this situation, we may just as well choose the most accurate method to compute quantiles, which is the local method. It can be carried out as indicated, but the effort can be reduced by employing an alternative scheme. Let $Q(\mathbf{s},\mu)$ be the quantile corresponding to the exceedance frequency μ with *fixed* strengths $\mathbf{s}$, than we compute $q(\mu^0)$ as

$$q(\mu^0) = \sup_{\mathbf{s}} Q(\mathbf{s}, \lambda - (\mathbf{s}-\langle\mathbf{s}\rangle)^T C^{-1}(\mathbf{s}-\langle\mathbf{s}\rangle)) \tag{5.26}$$

with λ chosen such that

$$\lambda - (\mathbf{s}-\langle\mathbf{s}\rangle)^T C^{-1}(\mathbf{s}-\langle\mathbf{s}\rangle) = -\log(\mu^0) \tag{5.27}$$

This scheme requires a similar computational effort as the scheme for computing a return period of failure, as both involve the combination of a search in the space of strengths and a line search to find the point where a real-valued function vanishes.

5.3 Adjustments to interface

It will be too complicated to take uncertainties into account in computing a design crest level corresponding to a fixed return period of failure. In fact, the option of design crest level computation is a rather exceptional item on the menu as it focuses on one particular parameter in the design of a dike, whereas a typical user would be concerned with various aspects of the design. For this reason, one might consider dropping this item; this would have the additional benefit that taking uncertainties into account can be offered for both remaining options "return period of failure" and "load quantiles". This would help keeping the interface transparent and simple. Otherwise, choosing the crest level design option should block the choice of taking uncertainties into account.

As remarked in 5.2.5, load quantiles cannot be computed for all output variables at the same time when uncertainty is being taken into account. Therefore, if uncertainties are to be taken into account in load quantiles, the user should choose the variable for which he or she needs a quantile; this is most elegantly done in a pop-up menu "Select Variable". This pup-up menu is deactivated (grey) when "take uncertainties into account" is off; then quantiles of all output variables can be computed.

Required output:	**Corresponding input:**	
Return Period of Failure	Safety Level (editable text)	
Load Quantile	Safety Level (editable text)	Select Variable (pop-up menu)

When uncertainties are taken into account, the user should indicate in which variables, and what are the statistics of these uncertainties. The variables can apply to

- Marginals;
- Wave model transformation;
- Structure and response of structure.

Variables who's values are *not* in the graphical interface should also be taken into account. This applies in particular to marginal uncertainties and uncertainties in wave transformations. A solution is to provide the options "Take uncertainty into account in:

- Marginals
- Wave transformation
- Structure and response of structure"

in the "Climate ands Reliability" screen. These options be selected using check boxes (nonexclusive). The first two options cause the program to take uncertainties in predetermined variables having predetermined statistics into account. Choosing the latter option, the user can still select uncertain variables and their mean values through the graphical interface ("Structure Screen").

For structure and response, variables and mechanisms considered uncertain can be checked separately in the "Structure Screen". For marginals and wave transformations, detail can only be specified "in the background", say in the editable ascii file "inpdata.m". We assume that a typical user is more familiar with the structural aspects of the problem than with hydraulics and extreme value statistics, as the models and estimates were prepared by specialists who have supplied sensible estimates of uncertainties in these. The user can change these values, however.

The editable ascii file "inpdata.m should also contain (co)variances for all possibly uncertain variables. The meaning depends on whether a variable is itself Gaussian, or its logarithm is Gaussian. If the logarithm of a variable is Gaussian, then the specified (co)variance applies to its logarithm. In the file, it should be clear which is the case by requesting a standard deviation either as a percentage (relative) or as a value of the variable (absolute, with proper unit). The value for a variable supplied by the user (either through the text blocks in the "Structure Screen" or through "inpdata.asc") is always supposed to correspond to a zero perturbation, whether the perturbation is of the variable itself (absolute) or of its logarithm (relative). Therefore, for variables already present in the current interface, mean values do not need to be supplied separately. New in the interface will be check boxes to indicate variables of the structure which are uncertain. These should be inactive if no uncertainty is taken into account.

The expressions for the various failure mechanisms may also contain random variables to account for uncertainty about the response of the structure. Recommended is to keep variances related to these uncertainties in the background (ascii file "inpdata.m"), so they are considered as part of the formulations for overtopping etc. It takes specialist knowledge about scale model experiments etc. to choose proper values. Values of standard deviations etc. are read from the ASCII input file so they can

be changed in the background. What the user can choose is whether uncertainties are taken into account or not for a particular mechanism, using a check box.

5.4 Presentation of estimates

Proposed is to present numerical output in the following form.

return period of failure without uncertainty:	
spread of return period of failure due to uncertainty (90% confidence interval):	[,]
return period of failure with uncertainty:	

Uncertainty in:	**Contribution to variance of log of return period of failure:**	**Fraction of variance of log of return period of failure:**	**Reduction factor of return period of failure:**
variable 1			
variable 2			
variable n			

5.5 Adjustments to computational modules

Possibly uncertain variables are collected in a single array, say beta_all. All elements of beta_all remain zero except possibly for those variables selected by the user as uncertain. The latter form beta (initially zero). Its elements are copied to appropriate elements of beta_all. Within the various modules, the operation

$$\mathbf{s} = \langle \mathbf{s} \rangle + C^{T/2} \beta \tag{5.28}$$

is always performed (whether or not a variable is selected as uncertain). It is assumed that nonzero correlation is only present between variables who's values are assigned in the *same* module.

5.6 Distribution functions of offshore loads

Proposed is to focus on marginals as according to theory (and provided asymptotic dependence is valid), dependence is much less uncertain than marginals. Marginal uncertainties still are a rather difficult problem. In particular, the dependence between marginal parameter estimates or quantiles of different (asymptotically dependent) variables is difficult to estimate.

A practical way forward for the short term could be a simulation study using e.g. Weibull distributions, involving the following steps:

- Specify dependence (parametric estimates from data) and marginal parameters (established estimates);
- Generate a number of data-sets of the variables, possibly longer ones for SWL;
- Estimate marginal parameters from data-sets;
- Examine joint sample densities of the parameters and of quantiles;
- Propose a model for these densities which is effective and as simple as possible (formulated in the smallest possible number of parameters, preferably one per variable).

6 Conclusions

- Overall, the marginal fits of wind speed and SWL for 12 wind direction sectors seem to match the data rather well (after correcting the omni-directional frequencies, see Section 2). As a function of wind direction, all parameters vary smoothly for both wind speed and for SWL.
- The directional marginals for wind speed at Vlissingen determined in this study may need to be improved upon later after applying appropriate corrections to the raw data which are dependent on wind direction.
- Wind speed and SWL coinciding with SWL maxima appear to be asymptotically dependent for wind directions in 225°-345°.
- This is good enough in practice to allow application of a semi-parametric method for estimating return periods of failure which is based on directional marginals. The results of this method look rather convincing.
- A local FORM-like approach to include various types of uncertainties about offshore climate, wave and sea level transformations, and the response of the structure into the semi-parametric method has been pursued further.
- It was shown how return periods of failure using this local approach can be split into factors corresponding to independent sources of uncertainty. This is relevant for reducing building cost by reducing uncertainty through additional research.
- Uncertainties can also be taken into account in estimating quantiles (values with specified return periods).

References

De Haan, L. and S.I. Resnick, 1977, Limit theory for multivariate sample extremes. *Z.Warscheinlichkeitstheorie verw. Gebiete* **40**, 317-337.

De Haan, L., 1990, Fighting the arch-enemy with mathematics. *Statistica Neerlandica* **44**, 45-68.

De Ronde, J.G., J.G.A. van Marle, A.P. Roskam and J.H. Andorka Gal, 1995, "Golfrandvoorwaarden langs de Nederlands kust op relatief diep water". *Report RIKZ/OS- 95.024 (in Dutch)*, Rijkswaterstaat RIKZ, Den Haag.

De Valk, C.F., 1994, "Selection of storm events and estimation of exceedance frequencies of significant wave height for five North Sea locations". *Report H1931*, DELFT HYDRAULICS, Delft.

De Valk, C.F., 1997, "Transformation of multivariate extreme value statistics from deep water toward the shore and calculation of failure frequencies for Pettemer Zeewering and Friesche Zeegat". *Report A26*, ARGOSS, Delft.

De Valk, C.F., J.G. de Ronde, J.A. van Marle en L. de Haan, 1998, "Assessing the reliability of coastal structures based on a multivariate description of the extreme offshore climate". *Submitted to Coastal Engineering.*

Ditlevsen, O. en H.O. Madsen, 1996, *Structural Reliability Methods*. Chichester: John Wiley & Sons.

Hasofer, A.M. en N.C. Lind, 1974, "An exact and Invariant First-Order Reliability Format". *J. Engrg.. Mech. Div. ASCE*, Vol. 100, pp 111-121.

Itô, K. (ed.), 1987, *Encyclopedic dictionary of mathematics*. The MIT Press, Cambridge, Mass.

Phillipart, M.E., Dillingh, D., and S.T. Pwa, 1995, *De basispeilen langs de Nederlandse kust - de ruimtelijke verdeling en overschrijdingslijnen*. Report RIKZ- 95.008 (*in Dutch*), Rijkswaterstaat RIKZ, Den Haag.

Rijkoort. P.J. en J. Wieringa (1983), *Windklimaat van Nederland*. Staatsuitgeverij, Den Haag.

TAW (Technische Adviescommissie voor de Waterkeringen), 1998, *Technisch rapport golfoploop en golfoverslag*. TAW, Delft.

Van der Meer, J.W., 1997, "Golfoploop en golfoverslag bij dijken". *Report H2458/H3051*, WL|Delft Hydraulics, Delft.

Van Vledder, G. Ph. (1998), "Demo Westerschelde - SWAN Golfberekeningen". *Alkyon Report A240*, Emmeloord.